THE APPLICABILITY OF FREE-FIELD ACOUSTIC SIGNATURES TO QUALITY INSPECTION OF ROTATING MACHINERY

by

Andrew Brattain Paustian

A thesis submitted to the faculty of
The University of North Carolina at Charlotte
in partial fulfillment of the requirements
for the degree of Master of Science in
Applied Energy and Electromechanical Systems

Charlotte

2016

Approved by:

____
Dr. Aidan F. Browne, Ph.D.

____
Dr. Wesley Williams, Ph.D.

____
Dr. Maciej Noras

ABSTRACT

ANDREW BRATTAIN PAUSTIAN. The applicability of free-field acoustic signatures to quality inspection of rotating machinery. (Under the direction of DR. AIDAN F. BROWNE)

Quality assessment tools are used to increase productivity of a production line by ensuring that the produced item is fit for consumer use. In order for a quality inspection tool to be useful, the process must not affect the item and should not significantly slow down the manufacturing process. Acoustic production can be quickly assessed in a non-intrusive manner and can depict significant information about the generation source. This thesis seeks to assess the usefulness of an acoustic quality inspection tool for rotating machinery and develop such a tool for a small air pump. The acoustics of several pumps were sampled and Fourier analyses were performed. Defects were introduced to the pump specimen and the acoustics were once again sampled. Comparing the divergence of a defective pump acoustic signature lead to the generation of a quality inspection prototype tool. An instrument was created and was able to diagnose two of the three selected pump defects based on its acoustic output. The third defect did not alter the pump acoustics but was still diagnosable by monitoring motor rotational velocity.

TABLE OF CONTENTS

INTRODUCTION

Purpose

The development of a production line has increased product yield tremendously, however, when assembling hundreds to thousands of components daily, oversights are inevitable. If a process in the production line results in the incorrect assembly of a component, either the lifetime or the functionality of the product may suffer. Quality checks are in place to identify any flaws in the product parts or assembly, ensuring that the produced product is in working condition. With the efficient nature inherent to a mass production process, a quality check can be a very lengthy step, slowing the manufacturing schedule considerably. The process becomes even lengthier when several tests are needed to check different parameters of the product's working state.

Unfortunately defective production line products are often missed and are distributed to the consumer, only to be returned shortly after for a replacement. To decrease the occurrence of defective product returns, an efficient and accurate way to detect flaws is necessary. The diagnostic tool would need to be able to assess variations of multiple parts of a finished product, and have a relatively short turnover time to move through a large quantity of products.

Many quality control techniques are used today to ensure that equipment is in working condition. Raišutis, Renaldas, et al review several different wind turbine inspection techniques including: vibration analysis, thermography, X-ray imaging, ultrasonic analysis and acoustical emission analysis. The usefulness of a specific testing technique can vary based on which defects they can identify and which are left undetected (Raišutis, Jasiūnienė, Šliteris, & Vladišauskas, 2008). To focus on defect detection that is non-intrusive to the product (will not harm the product in the inspection process) and can quickly pass or fail products off of a production line, the application of the test must be smooth and simple.

Acoustic emission analysis, or using acoustic pressure waves for the assessment of quality, is an ideal inspection tool. Acoustic analysis can be conducted one of two ways: passive and active acoustic analysis. An active acoustic analysis produces a known acoustic wave through the test subject and the reflection, attenuation and transmission of the noise is recorded and analyzed. A passive acoustic analysis technique relies on the processing of acoustic signatures that naturally occur, and analyzing how the natural acoustic signature differs from the expected signal (Raišutis et al., 2008). A passive acoustical analysis is ideal for quality control of a production line product because of its non-intrusive nature. The product functions at nominal conditions, and the acoustic spectrum is analyzed for variations.

The application of an acoustic analysis has been utilized by many different institutions including government labs, research facilities, in academia and in industry (Mba & Rao, 2006). With proven success and growing applicability in many different fields, acoustic emission analysis is a suitable tool for assessing product quality of mass produced goods. In an effort to further the development of acoustics as an inspection tool, the following research question has been developed: can different production line and assembly defects of a dual-diaphragm air pump be diagnosed using the analysis of the free field air coupled acoustic signature under standard operating conditions? It is the main focus of this thesis to seek an answer to the above question and develop a prototype quality inspection tool.

Answering the above proposed research question is not only of interest for industries producing pumps and other fluidic machinery, but also to companies producing products containing rotating machinery and “noisy” moving parts. If an acoustic assessment prototype does demonstrate success as a quality control tool, the instrument can be calibrated or programmed to address quality control of many other goods that are mass produced.

Acoustic analysis is an ideal tool for quality inspection because the tool measures something that is a standard byproduct of the machine, the machine does not need to be taken apart for testing and no external excitation is required. Some quality inspection tools rely on changes in the drawn current or voltage spikes. Though these methods can be successful at determining that something is wrong with the machine under test, it is difficult to pinpoint a specific defect. Acoustic output of a noisy machine can change with the slightest variance of mechanics. Acoustics are useful for pinpointing certain defects because of the vast differences that acoustic pressure can express. For example a 20 dBA increase in pressure propagating at 1000 Hz may signal that a valve is loose, while a 20 dBA increase at 10,000 Hz may indicate that the a faulty bearing was installed.

Another positive aspect of acoustic emission monitoring for quality inspection is the non-intrusive nature of the tool. Since the equipment under test never has to be broken down for inspection, the possibility of introducing additional defects is eliminated. Additionally, analyzing the noise without disassembly is much faster and easier than taking the test subject apart for a visual inspection; and even more so for large machinery.

Lastly, using passive acoustic inspection does not require external excitation or stimulus. X-ray and many forms of ultrasonic testing involve focusing waves and measuring the refraction and transmission of the waves through the machine under test. Passive acoustic analysis simply runs the machine under inspection and analyzes the acoustics. Furthermore, when analyzing air coupled acoustics there is no need for external sensors to be attached to the test subject. Most forms of vibrational testing require sensors to be mounted to the test subject increasing the required testing time. By utilizing air coupled acoustic as the testable phenomena the machine can undergo quality inspection as long a microphone is within the vicinity.

Background

Acoustical phenomena, or the production, propagation and detection of acoustical waves, are experienced constantly in the majority of people's everyday lives. Audible acoustic waves (pressure distortions propagating through a medium) fall into one of two categories: noise or sound. The main difference between noise and sound is the desirability of the acoustics (Carley, 2011). While noise is an unwanted phenomena, sound can be enjoyed or even utilized as a tool. An example using of acoustic waves as a tool is audible communication, or spoken language; an example of noise is static produced by a radio station that is not broadcasting.

Variation in acoustic waves generally refers to the differing frequencies or magnitudes of an acoustic wave. The change in frequency of a pressure wave is perceived by the human ear as pitch. A very high pitch acoustic wave corresponds to a very high frequency, while lower pitched sound refer to low frequency waves. The average human ear can detect pressure wave vibrations between 20 and 20,000 Hertz thought the ability to hear higher frequency content is degraded with age (Meyer & Neumann, 1972).

Variability in acoustic amplitude is how humans perceive what we refer to as volume. The human ear detects some frequencies better than others. A visual representation of the human auditory experience is displayed in Figure 1. Note that certain amplitudes of pressure waves at particular frequencies are audible to humans, while the same amplitude at other frequencies may be inaudible, as shown in Figure 1.

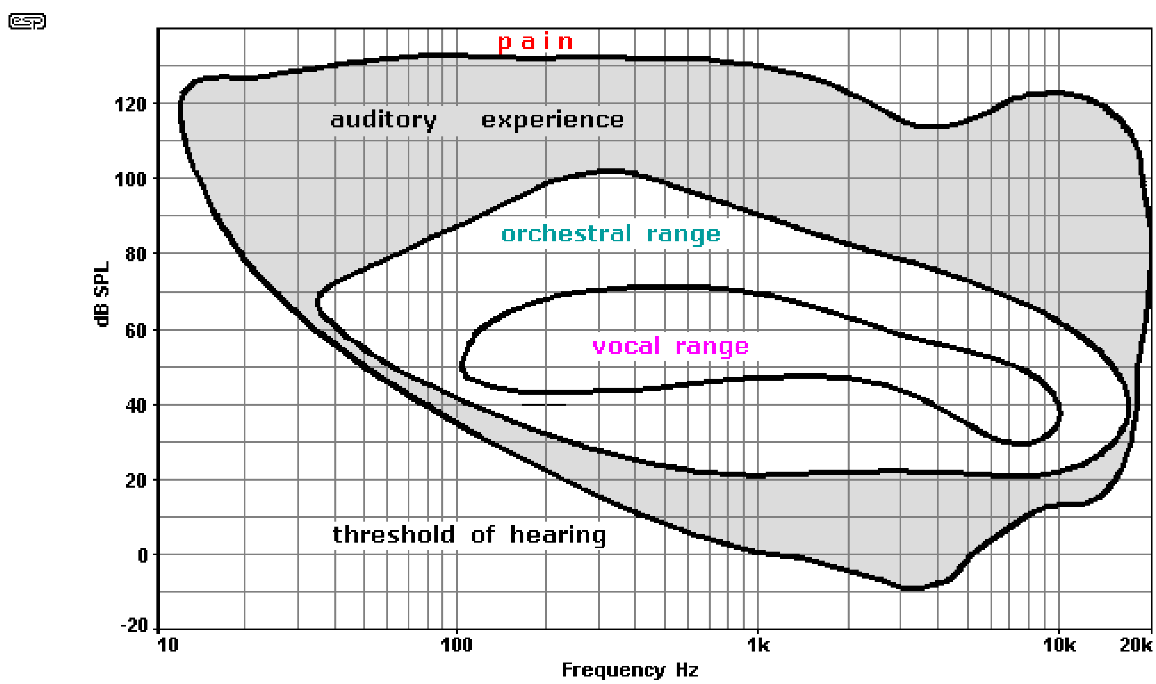

Figure 1: Human Hearing threshold (Elliott, 2006)

The Y-axis of Figure 1 is a measurement of the sound pressure level (SPL) and is scaled in the decibel. The decibel (dB) is a logarithmic scale that describes the magnitude of a certain occurrence, in this case air pressure waves, with reference to another occurrence. The accepted reference pressure is 2×10^{-4} μbar or more commonly understood as 20 µPa (Meyer & Neumann, 1972). The decibel is calculated using Equation 1. Where SPL is the sound pressure level expressed in dB and P_e and P_{ref} are the effective pressure amplitude and reference pressure amplitude respectively (Kinsler, Frey, Coppens, & Sanders, 2000).

$$SPL\ (dB) = 20log\left(\frac{P_e}{P_{ref}}\right) \qquad [1]$$

Modern acoustic transducers and instrumentation with high sampling speed, allows the detection of acoustic phenomena that otherwise might be inaudible to the human ear or overshadowed by greater magnitude acoustic waves. Using the improved sampling techniques an acoustic sample can be acquired and recorded for later processing. This time series data can them be transformed to view the acoustic sample as a frequency spectrum. This allows for the assessment of the different frequencies the acoustic sample contains. This process, known as Fourier analysis, provides an estimation of how much power is contained in individual frequency bands (Kinsler et al., 2000). A visual representation of the Fourier Transform concept is displayed in Figure 2.

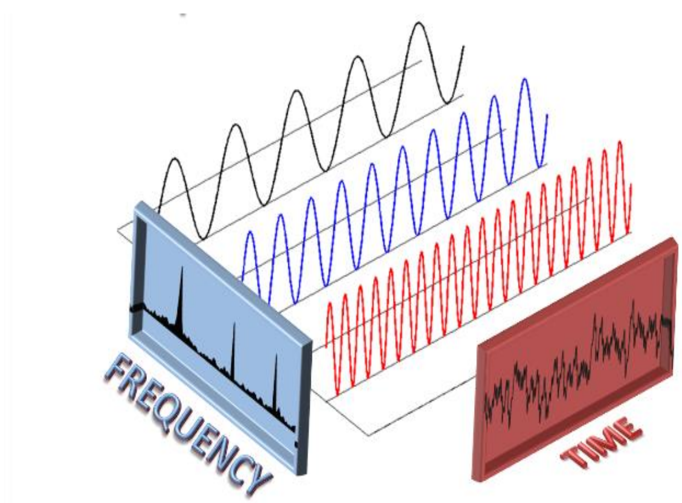

Figure 2: Illustration of Fourier Transform (Katabi et al., 2011)

The time series data is broken up into a series of its component sine waves; the amplitude of a specific sine wave at a certain frequency allows for the assessment of the power propagating at that frequency.

Thesis Statement

Based on my experience with acoustical emission, transmission and vibrational analysis gained on a project that characterized the acoustics of a dual-diaphragm, DC motor based air pump, I developed a hypothesis: passive acoustic emission analysis could be used to diagnose specific pump defects; and it could be done accurately and quickly without interfering with pump aesthetics, structure or function. Using generated acoustic wave variation a diagnostic tool could be created to assess pump quality based on nominal acoustic output. Analysis would be performed on several defects known to originate from the production line assembly. This tool could be designed and calibrated for the pump, and be altered to function for other reciprocating machinery.

Four main goals were to be accomplished during the thesis execution: (1) Diagnose three different pump defects based on the acoustic signature, (2) Note similarities in acoustic signatures for certain defects, (3) Design a prototype virtual instrument and test setup to diagnose pump defects introduced during the pump assembly, and (4) use a methodology allowing the tool to be easily adapted to inspect other machines.

LITERATURE REVIEW

Accurately classifying an acoustic signature and utilizing characteristics as a means of diagnosing defective machinery requires a knowledge of different areas of acoustics. To gain sufficient background in the acoustical field four general acoustic fields were investigated: generation, propagation, acoustic attenuation, and techniques/technologies used for acoustic signal processing. Additionally, literature was reviewed that directly related to acoustic pressure waves as a diagnostic tool.

Generation and Propagation

When seeking to use an acoustic signature for analysis of defects in a machine, it is helpful to have an understanding of what causes energy to be transmitted as pressure waves. Understanding how pressure waves originate can be useful when trying to identify what aspects of an acoustic spectrum are affected by certain machine defects. Two main acoustic generation sources exist in fluidic machinery: pressure waves induced from mechanical interaction and pressure waves induced from fluid flow.

Nigel Peake describes mechanical interaction as the primary acoustic generation source in his review of the challenges facing turbomachinery aeroacoustics. Peake states that the major generation source for aero engine noise is attributed to the fan interactions with the surrounding medium (Peake & Parry, 2012). A different mechanically induced sound that was investigated was the acoustics associated with friction. Rough surfaces sliding past each other develop stress fields when the crests or asperities slip while translating. This slipping action can cause energy to propagate as waves through the solid bodies that are experiencing friction (Akay, 2002).

The second type of generation source, the acoustics generated by turbulent flows, is detailed in Michael Carley's lecture notes on turbulence and noise. His notes not only provid a background on the concept of turbulent energy dissipation, but also link the turbulent flow pattern to the generation of acoustic waves (Carley, 2011). Carley's lecture notes provide mathematical models for generation source geometries such as point sources and spherical sources. Though most of the literature provided in the lecture notes centered around the link between acoustic wave production from turbulence, he also touches on noise generated from rigid surfaces such as the noise generated from a piston head (Carley, 2011).

Turbulently induced acoustic pressure waves are investigated by Marybeth Nored at al. in a report on compressor station piping noise. Nored et al. provide a recap on acoustic definitions and a short background on the theory of acoustics before stating that many times in compressor stations turbulently induced in compressor piping sound can make up the majority of acoustic energy (Nored, Tweten, & Brun, 2011). Flow induced acoustics can manifest in one of four ways: acoustics from fully turbulent flows, turbulent flows interacting with pipe geometry, acoustic and mechanical resonances excited by fluid flow, and vibrations of the pipe wall form turbulence or resonance. The report also details a number of planar and transverse waves that manifest in a fluid flow or a piping system (Nored et al., 2011). The article experimentally investigated the different acoustic oscillations generated while interacting with side branch geometry in piping systems. The acoustic oscillation frequencies induced were variable with the length of the side branch and were generated by the vortex action of the mean flow (Meissner & Czechowicz, 1995).

While assessing an acoustic signature, it is not only important to have an understanding of the generation sources, but also to realize how the noise is going to travel. Understanding the movement of a pressure wave is essential for an acoustic assessment. Certain defects could alter the transmission path of the pressure waves, affecting acoustic measurements. In order to ensure replicability between quality inspections, major transmission paths must be equidistant and in a geometrically similar position from the sensory equipment.

Alterations of how a pressure wave is predicted to act or sound, and how the wave actually propagates, are investigated in the 2008 Gas Machinery Conference by Dennis Tweten, Marybeth Nored and Dr. Klus Brun (Nored et al., 2011). They noted that the acoustic wave equations are limited due to assumptions; this led them to develop a new solver called the Transient Analysis Pulsation Solver (TAPS), which addressed the shortcomings of classical acoustic theory. The effect of including dynamic velocity and damping terms was tested against a standard acoustic wave equation (Tweten, Nored, & Brun, 2008). A large discrepancy was noted down the propagation path that Tweten, Nored and Burn attributed to the addition of the damping factor (Tweten et al., 2008). Because a compressor pressure pulse train is inherently similar to the pulse train associated with a diaphragm pump’s flow, predicting acoustic differences produced by mechanical defects is a challenge. Secondly, the TAPS solver findings expresses the importance of the pump position during testing. A large amount of energy is dissipated through normal propagation, stressing that the noise sources must be the same distance from the microphone.

A more general approach on acoustic propagation was published by J. E. Piercy and T. F W. Embleton who investigated the different interactions of sound broadcasting in the atmosphere. The review detailed many different environmental conditions that could have an effect on transmitted noise. The journal article covered the absorption of acoustic waves in various atmospheric gasses, the effect of wind direction and turbulence as well as the effects of topographical features like foliage buildings and elevation. (Piercy, Embleton, & Sutherland, 1977). When acoustic waves are in a similar medium such as the atmosphere the waves are referred to as free field acoustic waves, however, acoustic wave propagation acts very differently when interacting with acoustically reactive surfaces. Portions of the acoustic wave energy are reflected back to the first media and transmitted into the second media with every change in media that an acoustic wave contacts. The portions of the energy that are reflected and transmitted are determined by the density of the two materials, the angle of incidence and the speed that sound travels through the two materials (Kinsler et al., 2000). Because some materials reflect much more acoustic energy than they transmit (acoustically hard), acoustic wave propagation paths can be guided along material pathways or transmission lines (Meyer & Neumann, 1972). These transmission pathways often play an important role in how internal machine acoustics escape.

Attenuation

Classification of a flaw in a noisy machine based on the acoustic signature requires an accurate classification of how the machine sounds while operating both normally and defectively. To increases the repeatability between tests, acoustic signatures should not incur different levels of damping. In order to understand what may affect sampled pump acoustics, a knowledge of dissipative flow path geometries and acoustic attenuation devices is useful.

To ensure a precise measurement of the device under test, it is important to prevent outside unwanted noise from reaching the microphone. Good acoustic damping material is usually porous and dissipates incoming waves by means of friction. By varying the composition and layers of the porous material higher levels of attenuation can be achieved (Atalla, Panneton, Sgard, & Olny, 2001). The thickness of the porous material and the internal pore roughness and size all play a role in the dissipative properties of the material (Han, Seiffert, Zhao, & Gibbs, 2003). Acoustic foam or a similar medium can be used to dampen unwanted ambient pressure waves. It is also found that a micro perforated panel backed by an air cavity can more effectively attenuate lower frequency noise by means of mechanical resonance and cavity resonance. Using mechanical resonance of the cavity impedance plates, lower pitched acoustics can be attenuated at frequencies close to the natural frequency of the plates (Zhao & Fan, 2015). A prediction method for attenuation frequencies for such perforated absorbers was developed and tested to allow frequency attenuation to be chosen based on perforation diameter (Takahashi, 1997). A perforated material backed by a resonance chamber could also serve as a wall structure to block unwanted noise affecting the measured acoustics of a machine.

Attenuation of transmission paths must also be considered. If the majority of the acoustic energy is traveling down a defined transmission path, aspects of path can affect the signature, altering the produced acoustics. Geometries that have a known effect on acoustic signatures were investigated to ensure unaltered acoustics were sampled.

Common transmission path acoustic filters, such as a high pass, low pass and band stop filters, are introduced in the fundamentals of acoustics. A low pass acoustic filter takes the form of an expansion in the transmission path where as a high pass filter is a short open ended side branch (Kinsler et al., 2000). The dynamics of having a pipe attached to a transmission path could unintentionally incorporate an expansion chamber (or low pass filter) into the system. Overall, incorporating acoustic filters is not desired when sampling acoustic signatures, however, some filter geometries may be unavoidable in certain situations. An understanding of different filter geometries is required to ensure that non-altered signals are obtained between tests.

Another piping and component geometry that should be understood is the resonance chamber. Resonance chambers can be designed to stop specific frequencies from propagating through a path by altering the neck and volume dimensions of the chamber. A resonance chamber functions by producing destructive interference pressure waves back toward the noise source (Kinsler et al., 2000). Other studies have found that the maximum attenuation occurs when the generated pressure pulse is perfectly in phase with the source acoustic waves (Meissner & Czechowicz, 1995). Though resonation chambers and high/low pass filters are idealized to function with piped acoustics, many mean flow characteristics can alter how acoustic waves behave (Tweten et al., 2008). When this is true, the generation of pressure waves would not only fail to destructively interfere the oncoming waves but it would function as a generation source. While attempting to sample exclusively the unaltered acoustics of a machine, dissipative devices should be avoided. Resonators and inline restriction geometries have the ability to change acoustics and should be avoided when assembling the testing setup for the pump acoustic test chamber.

Acoustic Processing Tools

Breaking an acoustic signature down into frequency components is achieved through the processing time series data. One of the most important tools for spectrum analysis is the Fourier Transform. The Fourier Transform is similar to a Laplace transform in that it allows the processing of raw time series data to view a measured magnitude (acceleration, deflection, pressure) that is propagating at a certain frequency (Kinsler et al., 2000). While the Fourier Transform tool is useful for continuous signals, an analogous tool was developed for processing discrete sequences of data called the Discrete Fourier Transform or DFT (Weisstein, 2002) (Kinsler et al., 2000).

Though this process is useful for acoustic analysis, sampling a periodic signal over a fixed time interval can introduce error into the frequency analysis. If the sampling interval does not begin and end exactly in phase with the periodic acoustic pressure signal, the fragment of the period will be transformed into many different high frequency components. This phenomena is of energy in a certain frequency scattered into a number of different frequencies is known as spectral leakage ("Understanding FFTs and Windowing," 2015). To overcome the problems associated with spectral leakage a windowing function can be applied. Windowing functions assign a weight to different areas of time series data before a DFT is performed. By driving the partial cycles of a periodic signal to 0 the amount of energy that is “leaked” into other frequencies is minimized (Harris, 1978) ("Understanding FFTs and Windowing," 2015). An overview of different windowing functions and their corresponding time series data weighting can be reviewed in Harris' work (Harris, 1978).

Acoustics as a Quality Inspection Tool

Utilizing acoustic waves as a diagnostic tool is not a novel idea. Acoustic emission and propagation have been used in a large number of fields to assess problems ranging from mechanical deformations of wheels to partial discharge locations in electrical equipment. One such acoustic emission diagnostic tool was used on the exterior of piping systems to assess the amount of corrosion in a pipe during normal operating conditions (Hafizi, Nizwan, Reza, & Johari, 2011). Hafizi et al. conclude that using high frequency acoustic emissions excited by pressurized flow in the piping system could potentially determine the roughness of the pipes. It is also pointed out that a very high sampling rate is imperative to ensure that no flow induced emissions are undetected (Hafizi et al., 2011).

Acoustic emission is used to assess a wide variety of electrical components including transmission insulation failure and the quality of electrical circuit board components. In transmission and distribution systems faults can occur in the form of partial discharge. Partial discharge is usually resultant from a defect such as an air gap in the insulating layer that surrounds the conductor (Habel & Heidmann, 2013). Using acoustic emission can not only detect a partial discharge before a fault occurs, but the partial discharge can be pinpointed using a series of three or more acoustic energy sensors (Habel & Heidmann, 2013).

Acoustic emission has proven useful for a multitude of mechanical quality control processes. An advantage of using acoustic waves as a diagnostic or quality control tool is the use of passive acoustic assessment, or evaluating an acoustic signature of a machine that is normally operating. Using the passive acoustic signature of a machine, rather than exciting external acoustic waves, is desirable because the machine does not experience downtime during the inspection process (Raišutis et al., 2008). This technique is used to detect vibration occurring in wind turbine blades that indicate that mechanical wear is occurring and failure is imminent (Raišutis et al., 2008). Similar findings are discussed by Bin Lu, stating that acoustic emission is superior to vibrational systems at structural monitoring of wind turbines. The low operational speed of the turbine components make early warning diagnostics for mechanical vibration difficult; acoustic emission sensors can detect surface stress waves due to "rubbing action caused by failed components" (Lu, Li, Wu, Yang, & Applications, 2009).

Similar to acoustic emission diagnostics for electrical equipment, audio output can be used to pinpoint failure points in mechanical systems. Using a series of AE sensors allows for the detection of failure zones in wind turbines. Mechanically coupled acoustic energy sensors can detect acoustic events, or relatively large increases in acoustic output. Using two or more sensors allows the location of the events to be predicted. This technology can signal that failure is imminent when a large number of events occur in one location (Chia Chen, Jung-Ryul, & Hyung-Joon, 2008). Another example of locating defects of faults in a mechanical structure is assessment of the location of a failure in post-tensioned concrete structures, such as bridge cables. Again using a series of mechanically coupled acoustic energy sensors, a comparison of relative amplitudes of an acoustic energy can be conducted. Using sensor distance and the variation in detected magnitudes at the different locations allows for a calculation of the acoustic event source (Shiotani, Oshima, Goto, & Momoki, 2012).

Shiotani et al. were not only able to locate where the rupture occurred, but also noticed that two large spikes occurred during cable failure: one associated with friction of the breaking cable and the second attributed to the cable re-anchoring in the concrete structure. Furthermore, the secondary acoustic "re-anchoring" spike can be pinpointed utilizing frequency analysis (Shiotani et al., 2012). This finding provides evidence that specific characteristics of an acoustic signature can pinpoint different failure occurrences in a mechanical system. A similar technique called a time-domain distance transform is also a viable technique to pinpoint failure locations. Assuming that a failure produces a sufficient acoustic event, a series of AE sensors detect the time domain signals that are then reconstructed as distances using wavenumber-frequency mapping. Using multiple sensors allows the event location to be calculated (Grabowski et al., 2015). The time-domain distance technique is compared to a second technique referred to as the two-step hybrid technique. It uses predefined sensors and the propagation direction of lamb waves to determine an acoustic event source (Grabowski et al., 2015).

While acoustic event localization techniques are well developed and documented, there are relatively few publications on the determination of specific failures using acoustic signatures of operating machines. Diagnosing a failure of a functioning machine is slightly different from assessing the quality of a machine after production. The main divergence in the two assessments is that there is no failure acoustic event to detect using acoustic energy for the production line quality check. On the production line a single measurement does not have the benefit of a continual baseline, against which an event could be identified. A close parallel for acoustic quality inspection of a working machine can be made with an acoustic device that detects defects in train wheels when a train passes over certain sections of tracks (Bollas, Papasalouros, Kourousis, & Anastasopoulos, 2013). The train is diagnosed when operating under normal conditions, thus eliminating time to be set aside for inspection. While other tests require the application of specific conditions, the acoustic diagnosis of train wheel defects can occur while the train is operating under normal conditions. This correlates to the application of acoustic diagnosis of a pump specimen because the pump can be assessed while operating under normal conditions.

The sparseness of acoustic defect investigation for a running machine operating under nominal conditions may be resultant of the vast differences of acoustic signatures for different defects in varying types of reciprocating or rotating machinery. The amount of possible defects that could alter the standard acoustic signature of any given machine is so large that individual studies must be performed on specific machines to be of use to the manufacturer as a quality control tool. An assessment of the viability of such a tool on a reciprocating dual-diaphragm pump is detailed in later sections.

DESCRIPTION OF EQUIPMENT

Test Setup

To generate a quality assessment tool of a certain machine requires a preexisting knowledge of the machine's acoustic signature. Using the acoustic signature of healthy pumps provides a baseline to which unhealthy pump acoustics can be compared. To ensure that changes in defective pumps acoustics can be identified, it is vital to ensure that unwanted noise does not contaminate the acoustic signature. If this is successfully done, differences in the pump acoustics can be accredited to the introduced defect.

A lab bench testing environment was created to facilitate the capture of pump acoustics. This setup can be viewed in Figure 3. Each pump (represented by the red rectangle) was suspended in a foam test chamber during the testing process. The Inlet and outlet tubing and electrical leads were fed through the back of the testing chamber. The outlet was plumbed to a back pressure regulator, and the inlet was secured to the front of the test chamber. The microphone was inserted into the chamber through a small port on one side of the chamber. Figure 3 displays the test chamber without the front cover to display the internal setup. Appropriate instrumentation was used to acquire and process sound pressure level and motor rotational velocity data. A detailed description of the equipment that was used for testing is included in the following section.

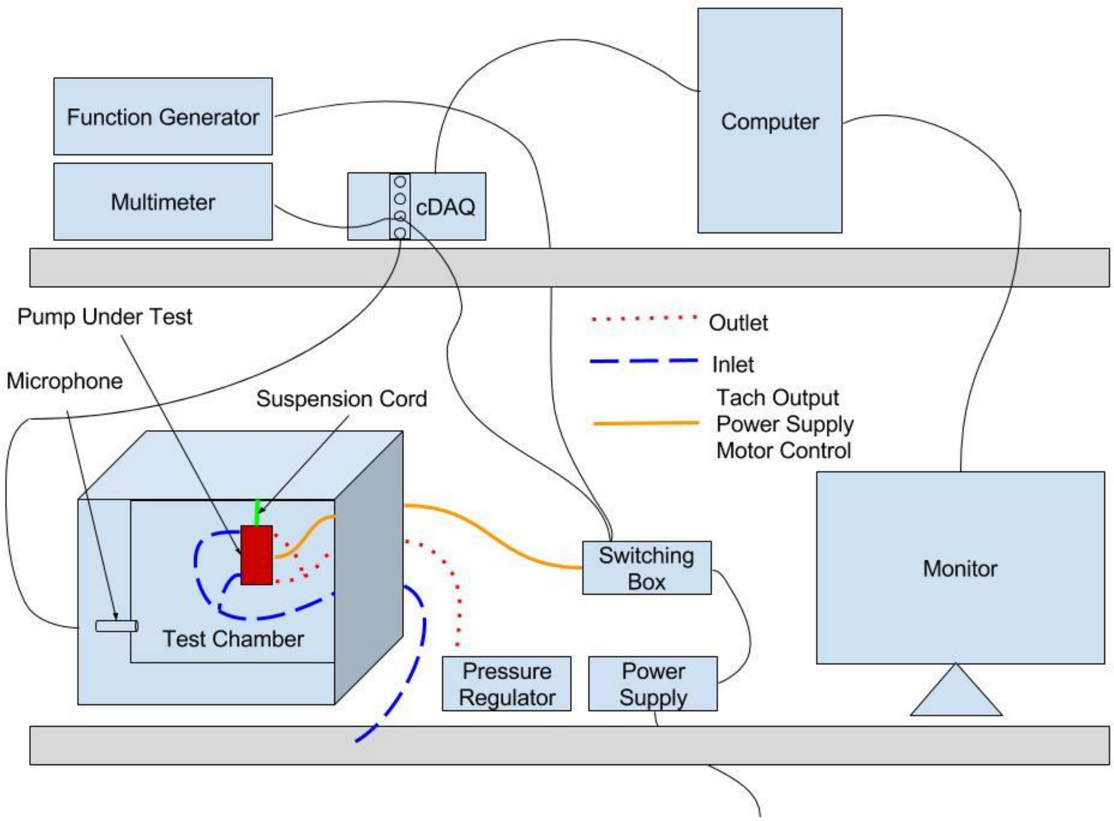

Figure 3: Lab bench testing environment

Physical Equipment

The acoustic signals were sampled using a Brüel & Kjær Type 4936 free field microphone equipped with a Brüel & Kjær Type 2671 preamplifier. The microphone is ½ inch with a prepolorized condenser type backplate. The microphone was able to detect sound across the entire acoustic spectrum of 20-20,000 Hz. The free field response frequency band was flat between 10 - 10,000 Hz with a drop off of 3dB of sensitivity between 10,000 to 20,000Hz and from 3 - 10Hz. The frequency response curve is included as Figure 4.

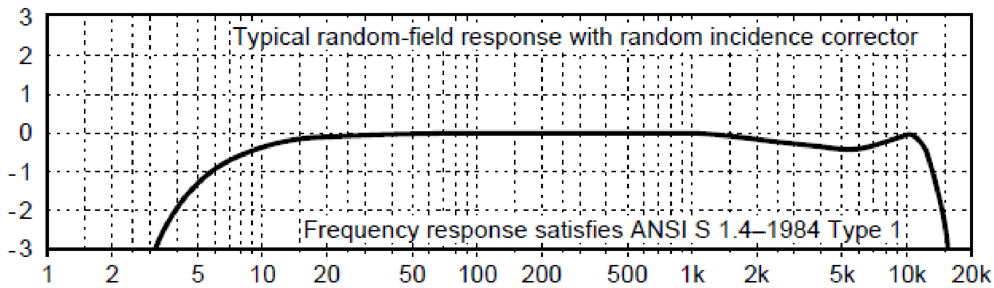

Figure 4: Microphone Frequency Response Curve (Bruel & Kjaer)

The microphone sensitivity was tested using National Instruments Measurement and Automation Explorer (NI MAX) and a 3M acoustic calibrator. The calibrator produced a 114 dB spike at 1000 Hz, NI MAX software then correlated the microphone voltage response to the known SPL input. The microphone sensitivity was measured to be 40.9 mV/Pa which was a verified shift from the manufacturer supplied sensitivity of 40.4 mV/Pa. The microphone had a wind screen placed over the top to reduce ambient acoustics. NI MAX was also used for the sensitivity measurement.

The preamplifier was connected with a BNC type connector to the data logging device. The frequency response of the preamplifier was +/- 0.2 dB across the band of interest. The preamplifier was supplied with 2mA excitation current. The maximum output of the preamplifier was a 7 volt peak corresponding to approximately 141 dB according to specifications. The microphone preamplifier sampling task was set up using National Instrument Measurement and Automation Explorer. The acoustic measuring system was set to measure continuously and to convert the raw pressure measurements to the commonly used decibel with 20 µPa used as the reference pressure. The preamplifier microphone combination can be viewed in Figure 5.

Figure 5: Preamplifier microphones assembly

The logging device that was used was National Instruments Compact Data Acquisition System (cDAQ) with four port chassis model number 9174. In the first port of the cDAQ, a NI 9234 analog input 4 channel module was installed. Figure 6 is an image of the cDAQ chassis and 4 channel module.

Figure 6: cDAQ and 4 channel module

The NI-9234 module is able to sample up to 51.2 kS/sec on all four BNC connectors. The cDAQ was connected to a computer with LabVIEW using a USB cable. The computer had an Intel Core i7-4810MQ processor clocked at 2.8 gigahertz, and 16 gigabytes of memory. The microphone/preamplifier assembly was connected to port 2. Port 3 sampled the tachometer output of the pump to assess the rotational speed of the motor.

The tach output of the pump (blue wire in Figure 7) was connected to a BNC tee splitter at the input port to the cDAQ module. The other end of the tee was connected to a digital Agilent 34401A 6 ½ Digital Multimeter (used in frequency measurement mode) to determine the real time rotational speed of the pump before and during the testing periods. A speed control circuit was incorporated in the pump motor to drive the pump at varying speeds. The speed control circuit input was incorporated in the wiring to the pump motor. The complete motor connector with wire description can be viewed in Figure 7.

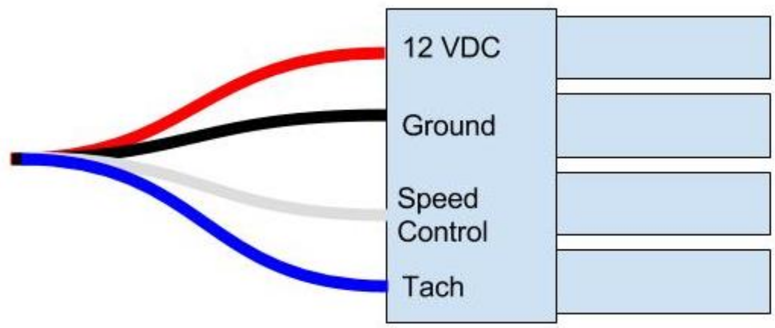

Figure 7: Motor connector diagram

The speed control lead for the pump was connected to a Tektronix AFG 3102 Function Generator to produce a pulse train with a variable duty cycle for controlling the pump motor rotational speed. The function generator and multimeter can be seen in Figure 8 below.

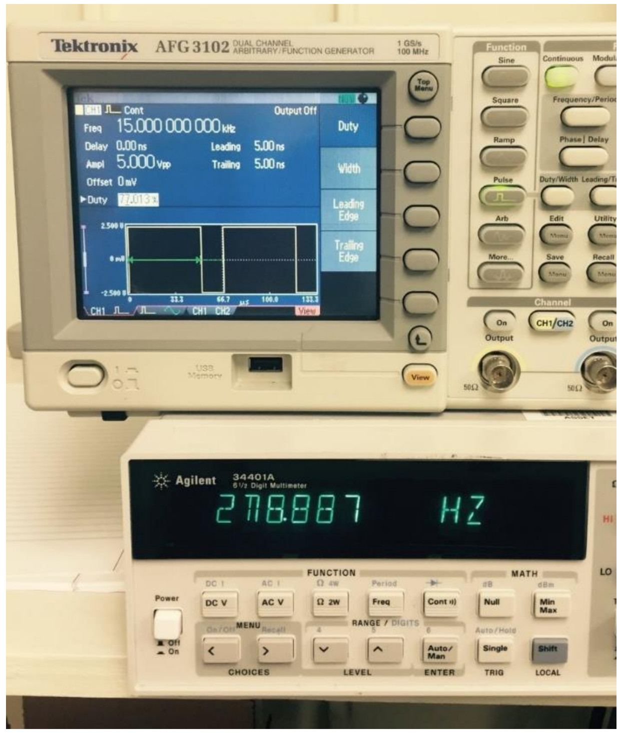

Figure 8: Function generator (top) multimeter (below)

The pump was supplied power by a Micronta Regulated 12v power supply. The mechanical components of the pump testing tool consisted of a back pressure regulator, vinyl tubing, a power switching box and a foam chamber for ambient acoustic dissipation.

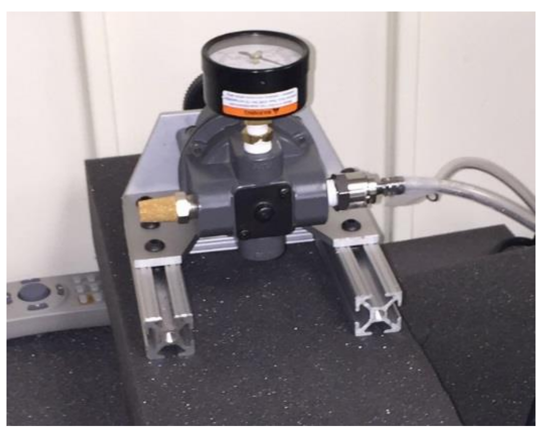

Figure 9: Back pressure regulator

The back pressure regulator was a ControlAir Inc. Type 700BP which was connected to the flow output of the pump using the vinyl tubing (Figure 9). The diaphragm pump operated with two heads each containing an inlet and outlet on either side of the pump. Two short (3 inch) vinyl segments were connected to outlets and then connected to a Tee pronged plastic vinyl tube connector. The pump port layout can be viewed in Figure 10. The tubing arrangement can be viewed in Figure 11.

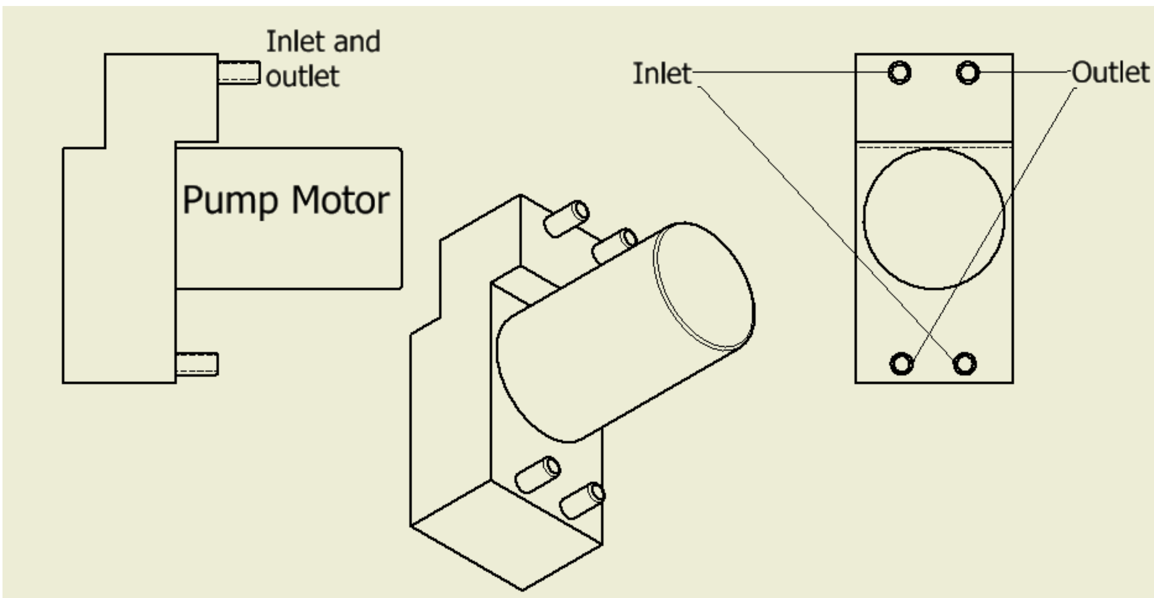

Figure 10: Pump inlet and outlet arrangement

The third side of the connector was piped to the back pressure regulator using a 2 foot piece of vinyl tubing. The inlet layout was similar to the outlet except the third longer piece of tubing was secured to the outside of the testing foam chamber instead of a pressure regulator. The vinyl tubing used was 3/16 inch ID and 5/16 inch OD. The foam chamber dimensions were one foot by one foot by one foot; it was constructed of packing foam. The chamber relied on the foam walls for support and pinned at the corners to hold the structure together. A foam front panel placed over the opening of the chamber during testing but was removable to access the pump specimen. An image of the open testing environment can be found in Figure 11.

Figure 11: Foam test chamber

Figure 11 also displays the orientation in the chamber of the microphone, vinyl tubing, pump wiring and suspension cord. The cord was threaded through a small hole in the roof of the chamber and used the rigidity of the chamber as support. The power lead and the inlet and outlet tubes were negotiated through a corner of the testing chamber (view Figure 11). The inlet tube was secured to the front of the chamber and the outlet tube was connected to the back pressure regulator.

LabVIEW Prototype Sampling

A virtual instrument was created using LabVIEW 2014 and its provided library functions to transform time series data into power spectrum data. NI Max was used to set up the sampling criteria for the microphone. A sampling task was created to acquire

51,200 pressure samples every second from the microphone. The LabVIEW instrument was set to obtain 200,000 samples of sound pressure. With a sampling rate of 51.2 kHz the obtained period was over a duration of approximately 3.91 seconds (refer to Equation 2). The frequency resolution of the resultant FFT was 0.256 Hz based on the sample acquisition speed (refer to Equation 3).

$$Sampling\ period = \frac{number\ of\ samples}{sampling\ frequency} = \frac{200{,}000 samples}{\left(^{51{,}200 samples}/_{second}\right)} = 3.91 seconds \qquad [2]$$

$$Frequency\ Resolution = \frac{1}{sampling\ period} = \frac{1}{3.91 seconds} = 0.256 Hz \qquad [3]$$

With 51,200 samples taken per second the Nyquist frequency, or the maximum frequency that the FFT tool can measure is 25,600 Hz ("FFT Fundamentals (Sound and Vibration Measurement Suite)," 2009). The virtual instrument also acquired the rotational velocity of the pump motor. The speed data was averaged to determine motor rotations per second during the trial.

It was decided to apply an A-weighting to the acoustic data to portray the frequency spectrum that the human ear detects. The resulting decibel levels sampled by the microphone were recorded as dBA to indicate that a weighting was applied. A Fourier analysis was then preformed on the acoustic data. No averaging was applied to the data. The option exists to apply zoom settings for the data, however it was desired to observe the full acoustic spectrum, therefore, no zoom settings were used.

A Hanning window was applied to all time series data to decrease the effect of spectral leakage. Spectral leakage is an artifact created from Fourier analysis; incomplete periods of sampled acoustic pressure result in portions of the acoustic energy that appear under a different frequency. Eliminating the incomplete frequency content results in frequency domain data without frequency artifacts. ("Understanding FFTs and Windowing," 2015). After the FFT tool assessed how much power is propagating in different frequency bins, the data was reported as a cluster of 3 elements: cluster element number, frequency step and the associated magnitude of the sound pressure level. The sound pressure level magnitude for each sample index corresponded to a frequency calculates as the product of the element number and the frequency step. The cluster of elements is then plotted on a waveform chart to visually show the acoustic signature. An example of the LabVIEW front panel can be found in Appendix 7.

METHODOLOGY

Pump Defecting Procedure

The manufacturer of the pump has characterized common defects that occurred during the assembly procedure. Some defects are identified by current quality inspections and some are identified when the pump is returned. Three pump defects from this list were selected for developing the new diagnostic tool. The defective pumps from the production line were never used, the defects originated in the manufacturing procedure or through the use of defective parts. The defects that were chosen for acoustic signature assessment are: a pump assembled with a diaphragm containing a hole, a pump assembled without a washer on the diaphragm and a pump that was assembled with two diaphragms instead of one.

In order to develop a diagnostic tool that can accurately determine a pump's quality based on the acoustic signature, there must be a forensic investigation of defective pump acoustic signatures. The defective signatures must me compared against each other to define repetitive characteristics. The signatures should then be compared against spec pump acoustic signature to determine divergences resultant of the defect. Once acoustic abnormalities can be accredited to specific defects, logic can be applied to develop the automated tool.

The diaphragms containing the holes were created based on a sample defect pump supplied by the pump manufacture. The observed hole in that pump was a 3 mm rip in the diaphragm that was exposed when the pump head was removed. An investigation as to where the hole position should be with respect to the pump outlets was carried out in order to create the most representative device for testing. The angular position of the diaphragm hole that produced the acoustic spectrum with the least amount of change from the pump assembled to specification determined the position of the hole for future testing. The angular position investigation was carried out to be able to diagnose pumps with holes in their diaphragm regardless of their position; by choosing the position with the least about of variation, other hole in diaphragm positions will also fail the quality inspection. Eight different diaphragms were punctured to produce tears similar to the supplied hole in diaphragm pump. The pump head was removed and the diaphragm was removed and was replaced with a random defective diaphragm. The head of the pump was reinstalled for testing.

The missing washer defects and the double diaphragm defects are quality checks not for the assembly materials but assembler compliance with assembly procedures. Both defect circumstances have been observed in production line pumps. The missing washer most likely results from employee fatigue from repetition, as you can visibly see if the washer is in place before the pump head is attached. The washer was removed and the pump head was then reattached to the now defective pump specimen.

Another human introduced assembly error is when two diaphragms are mounted on a single side of the pump. When the employee selects a diaphragm to install onto the piston arm pump some of them are perfectly stacked so the only observable difference is the diaphragm thickness. If two diaphragms are incorporated instead of one, the pump functionality may suffer. To introduce this defect into the pumps the diaphragm is removed and replaced with two nested diaphragms. The pump head is then reattached to the pump.

Testing Procedure

To begin acoustic testing of a pump specimen the acoustic dissipation chamber was opened and the pump under test was hung from the suspension cord. Measures were taken to ensure that the testing environment was clear of unnecessary acoustics by powering off any other electronics or fans. The pump's 4 ports (2 inlet and two outlet) were then connected to vinyl tubing in the arrangement described in the equipment description section. The power lead for the pump was connected to the power supply switch.

With the pump secure and all pump tubing and wires in place the procedure began a four part process. First the pump was supplied power and the rotational velocity was allowed to settle for around 10 seconds (viewed using the multimeter frequency display). The first acoustic test for each pump specimen was with the pump operating without speed control pumping air against 12 psi back pressure. The virtual instrument was run and the data saved.

The second part was testing the same pump under the same back pressure (12psi) with the speed controlled. The function generator that connected to the pump speed control port was activated. The generated function was a square wave that was set to 15 kilohertz with an amplitude of 5 volts peak to peak with zero DC offset. The speed of the motor was controlled by varying the duty cycle of the pulse train produced by the function generator. The pump motor was then driven to 45 rotations per second and the second run of the virtual instrument was initiated.

The third part was with the pump's speed controlled but with the pump operating at ambient pressure. The acoustic dissipation chamber was opened and the pump tubing leads were disconnected from the 2 inlet and 2 outlet ports. Once the tubing was disconnected the pump suspension cord was altered to maintain the proper orientation of the pump with respect to the microphone. The pump was supplied power. The generated function's duty cycle was adjusted to drive the pump at 45 Hz. The chamber was closed and another signature was sampled by the virtual instrument.

The fourth and final part of the testing procedure for a specific pump arrangement was the pump operating at ambient pressure with the motor running without speed control. The function generator was simply deactivated and the virtual instrument was run to collect an acoustic signature.

The next specific pump was then placed in the acoustic chamber for testing. Pumps 1-6 were all tested in order with the same defect on the same side of the pump to keep track of which defects were in place. Due to the large amount of time that is required to disassemble pumps, introduce defects and reassemble pumps according to the manufacturer's specifications, each specific pump, after assembly, was tested with the 4 part procedure to collect all data before having to disassemble, fix the defect, and reassemble. An example of a single specific pump that was tested using the four part process is Pump 1, with a hole in the diaphragm on side 1. Pump 1 with a hole in the diaphragm on side 2 would be considered a separate configuration. After all 6 pumps went through the full testing procedure the pumps were disassembled and reassembled with the new defect position or new defect type.

LabVIEW Diagnostic Process

After the time series data is transformed into frequency data using the previously described LabVIEW Fourier analysis tool, the data is structured as a cluster of three elements. The data is displayed as a spectrum plot to show a visual representation of the power spectrum on the front panel and also is indexed for assessment of variation from standard pump acoustics. If certain locations show significant amount of variation the tool will diagnose a defect in the pump under test. The cluster is then unbundled into individual array. The magnitude array is split into separate sub arrays containing the starting point of the frequency assessment location and the bandwidth of the assessment. Based on the experimental data for defects certain frequency bands contained more acoustic power than others. As an example of the acoustic signature location assessment Figure 12 displays example locations that the tool would index for comparison. To perform a threshold assessment over the area covered by the red box in Figure 12, the array cluster number is calculated as 3906 (Equation 4).

$$\frac{frequency\ of\ interest}{frequency\ step} = \frac{1000\ Hz}{0.256\frac{Hz}{cluster}} \approx 3906^{th}\ cluster \qquad [4]$$

The 3906th cluster corresponds to a frequency of 999.94 Hz, and can be used as a starting point of the analysis.

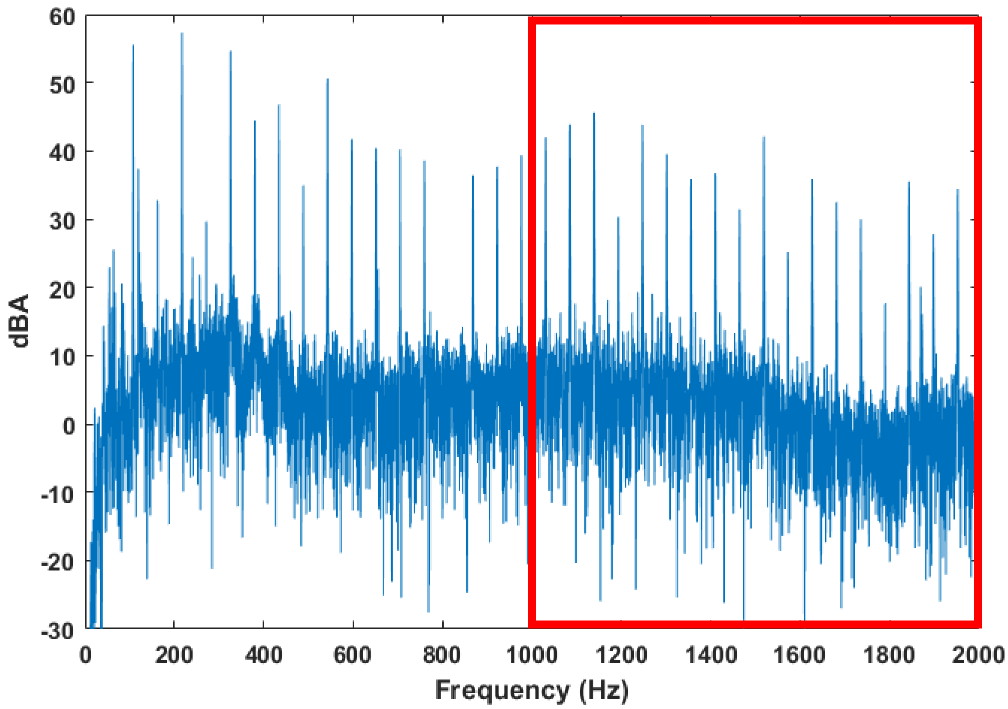

Figure 12: Example area for acoustic indexing

For certain evaluations the assessment location varies; it is correlated to the rotational speed of the pump for that particular run. For variable locations, thresholds were set for sub array bands of interest. The threshold was set to identify when the amount of energy in the band was significantly above average. If more acoustic energy is propagating in certain frequencies of interest, the diagnostic tool will indicate that there is a specific defect present in the pump under test. The quality check will pass or fail certain pumps by assessing the number of individual frequency magnitudes above the threshold for a pump to model specifications. If the number of peaks above the threshold value exceeded a set amount the pump would fail the quality check.

A secondary diagnostic method was developed for assessing pump quality. An averaging tool was generated to view the total power in certain sections of the acoustic spectrum. The averaging tool was implemented at a set frequency band of interest. Unlike the threshold tool described above that assesses peak magnitudes, this averaging tool assesses total acoustic power over a band of interest. While some pump flaws increase high magnitude peaks, others cause an upwards shift of lower magnitude acoustic data over a range. This phenomena is easily captured using a frequency range average as the large spikes were only a portion of the overall acoustic energy in the averaged range. If the acoustic energy between the large spikes is of higher magnitude than a signature with the same acoustic spikes but lesser acoustic energy between spikes, certain pump defects can be diagnosed.

RESULTS

MATLAB Enveloping Tool

Plotting several sets of acoustical data in a single figure can quickly become crowded. In order to highlight the important aspects of an FFT plot, an enveloping tool was used. To isolate significant peaks, a MATLAB function named findpeaks was used. This tool breaks a FFT spectrum graph into significant peaks, labeled Peaks1, and the corresponding frequencies, labeled Freq1. The developed code is set to take all of the information in the first vector of the Pump matrix and designate significant peaks. The corresponding frequencies were recorded for each significant peak to ensure the FFT shape was preserved. The resultant plot was a display of the top SPL values of the spectrum.

Finding the peaks decreased the amount of data for each plot, however, the number of peaks was still far too great for multiple plots in a single figure. The distance between peaks is set using the MinPeakDistance. This ensured that after a peak was located there would have to be a minimum of 45 Hz before another peak was located. 45 Hz was chosen because the speed of the pumps was limited to 45 or higher. The acoustic signatures of the pumps contained large spikes that appeared as multiples of the rotational frequency. Separating the find peaks function by 45 Hz allowed for the pumps major peaks to be separated from other lesser peaks. Using the enveloping tool, with the added MinPeakDistance criteria, decreased the pump FFT data from 78086 data clusters to around 360. An example of how the enveloping tool works is included in Figure 13.

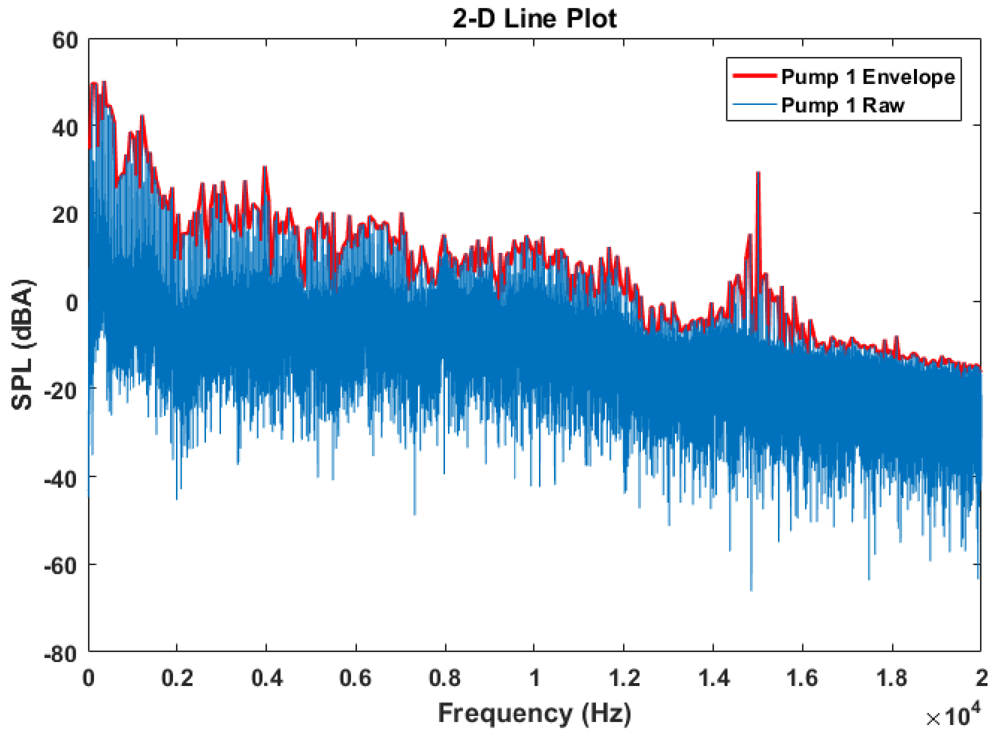

Figure 13: Pump 1 Envelope vs Raw Data Example

The application of the enveloping tool displays a plot of just the significant peaks of the FFT. Though both plots in Figure 13 may adequately show the trends of the FFT, the enveloping tool is useful when plotting several acoustic signatures in the same figure. Unless otherwise labeled, Plots containing 6 pump comparisons and comparisons of defective and standard pumps have had the significant peaks highlighted and will be referred to as envelope plots. The enveloping tool is only used as a means to clearly highlight acoustic similarities and differences. The acoustic diagnosis prototype tool that was developed assessed pump quality using the raw pump signature. The MATLAB code that was used can be found in Appendix 8.

Pump to Specification Comparison

Pumps assembled to manufacturer specifications (spec pumps) were tested to determine a baseline of the acoustic spectrums. As detailed in the methodology section the 6 spec pumps were tested under the four operating conditions. This spec pump data can be viewed in Figure 14 through Figure 17.

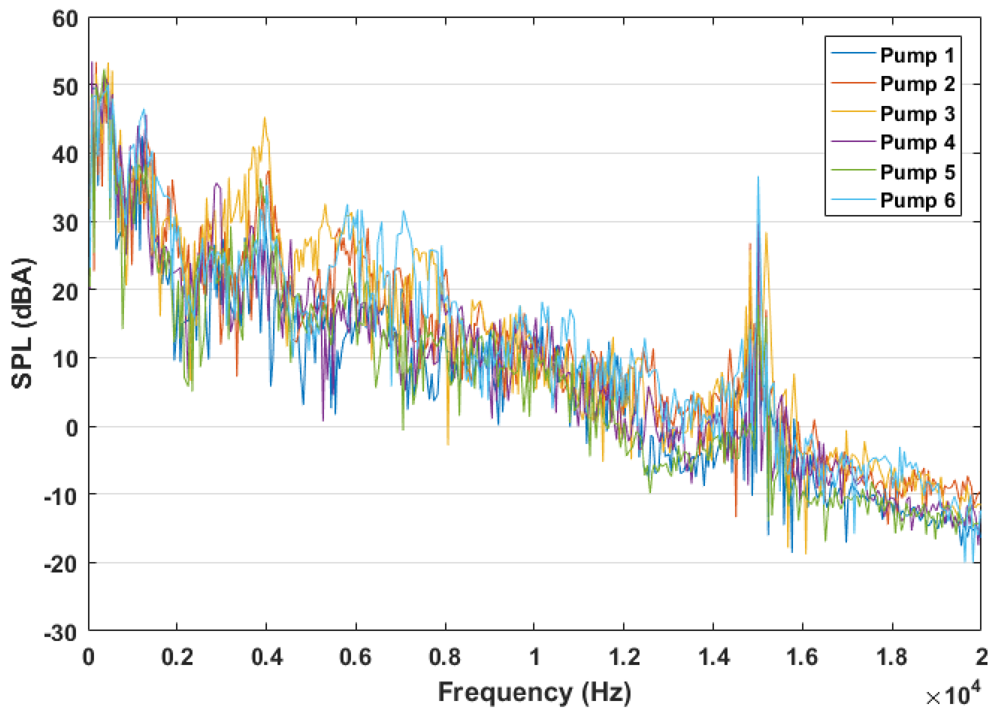

Figure 14: All spec pump comparison under 12 psi back pressure speed controlled

Figure 14 displays all 6 spec pumps under 12 psi back pressure with a motor rotational speed of 45 Hz, the tolerance on this setting for all testing was +/- 0.1 Hz. The maximum acoustic pressure magnitude was slightly less than 55 dBA. A secondary acoustic spike was noted between 3000 and 4000 Hz with a lesser magnitude of 45 dBA. The spikes in the envelop plots that appear at 15 kHz were resultant from noise introduced to the ac output of the mic. The 15 kHz noise is attributed to the function generator that is used to vary the rotational speed of the pump. Though the spec pump signatures in Figure 14 do exhibit variability, the overall trends of the pump were very similar between trials.

The majority of the acoustic energy appears to be propagating at lower frequencies bellow 600 Hz. Past testing on the pump under test has indicated that the majority of this noise is due to the mechanical components of the pump (Browne & Paustian, 2016)**.** They found that the major acoustic spikes in this range propagated as multiples of the diaphragms' actuation speed (which equates to even multiples of the motor rotational frequency). The frequency range of 600 Hz to 20 kHz was attributed to the aeroacoustical interactions of the flow path. This conclusion was met because there is a lack of vibrational energy at this frequency range that would be present in mechanically induced noise. There was far less acoustic energy associated with the air flow than the actual mechanical components. The same observations were made in the current testing. It should be noted that pump 3, in yellow, produced slightly higher acoustics in the secondary spike than other similar pumps. This behavior is viewed between 2000 Hz and 6000 Hz of Figure 14.

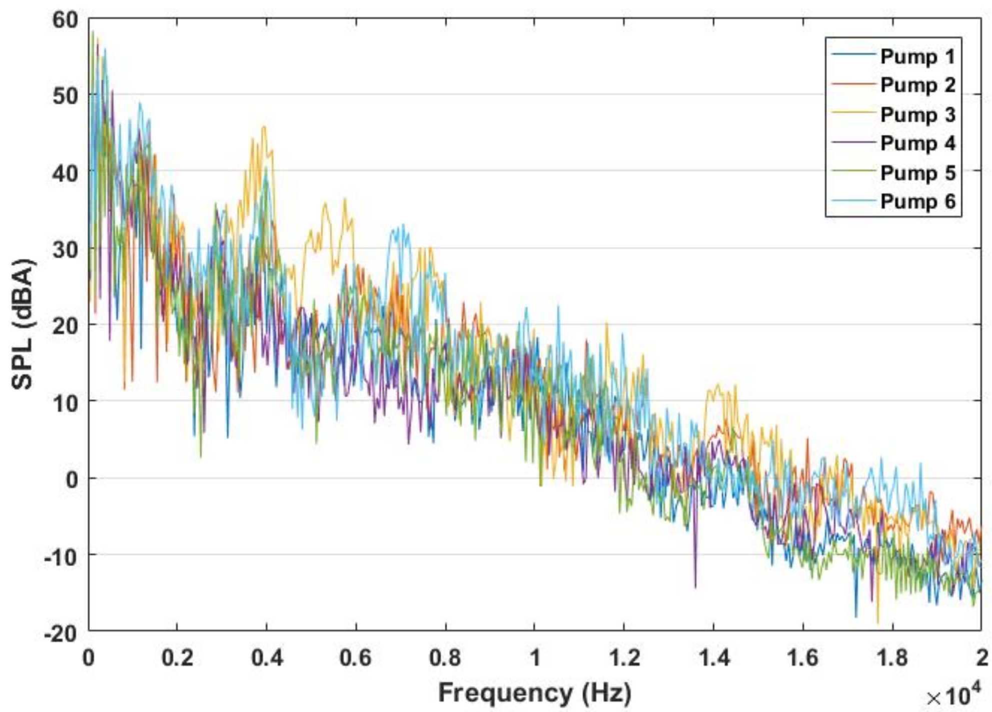

Figure 15: All spec pump comparison under 12psi back pressure speed not controlled

Figure 15 shows the envelope plot of the 6 spec pump specimens operating under 12 psi back pressure without motor control. The motor rotational speed was variable with values between 53.83 Hz to 55.15 Hz. While similar in shape to Figure 14, the spike at 15 kHz does not appear due to the motor operating without speed control. The frequencies with the greatest acoustic spikes in Figure 15 occur in the mechanical range and have magnitudes between 55 and 60 dBA. The secondary acoustic spike was also produced by the 12 psi no speed control pump tests. The magnitude was also less than the primary acoustic spike topping out between 38 and 45 dBA.

The overall trend of both of the spec pump under 12 psi back pressure plots is decreasing pressure magnitudes with increased frequency. The elevated acoustics of pump 3 were also noted in the 12 psi not controlled spec pump tests between the ranges of 2000 to 6000 Hz in Figure 15.

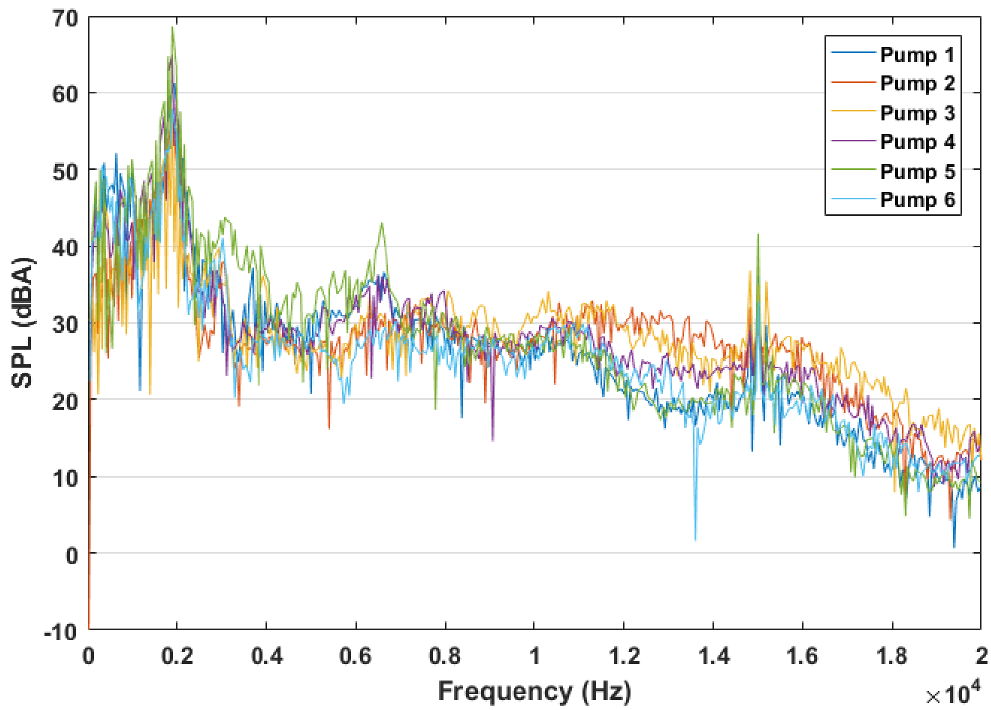

Figure 16: All spec pump comparison under ambient operation speed controlled

Figure 16 shows the envelope plot of 6 spec pumps' acoustic signatures operating in ambient conditions with the speed held at 45 Hz. Similar to Figure 14 the 15 kHz motor control noise spike is visible. The pump operating under ambient pressure did not have the same loading as a pump that was moving air into a pressurized environment. The acoustics of the spec pump under ambient conditions achieved a slightly higher acoustic output compared to pump with backpressure. With a maximum magnitude of just under 70 dBA, the slightly higher acoustic signature was due to the acoustic propagation of the pump being contained inside the test chamber as opposed to transmitted out.

The large acoustic spike of 60 to 70 dBA that is noted just below 2000 Hz is not observed in the trials with 12 psi back pressure. Though other acoustic spikes developed in some pump tests during the ambient speed controlled test, there was no consistent secondary spike as seen in Figure 14 and Figure 15. Figure 16 also displays how the noise floor is much higher in acoustic tests without back pressure. The frequency range of 18000 Hz to 20000 Hz has pressure waves centering around 15 dBA, while Figure 14 and Figure 15 have pressure ranges centering around -10 dBA over the same frequency band. The increase in the acoustic noise floor for the ambient tests was also attributed to the lack of air plumbing into and out of the test chamber. When the air was not pumped outside of the chamber the higher frequency content that was muffled by the foam chamber was more detectable for the microphone. The higher frequency acoustic waves were less detectable to the microphone when the transmission path lead out of the chamber. High frequency acoustics incur greater dissipation through porous material than lower frequency content (Atalla et al., 2001). This resulted in the lower end of the pump spectrum being detected during the 12psi testing but the higher frequency content was damped.

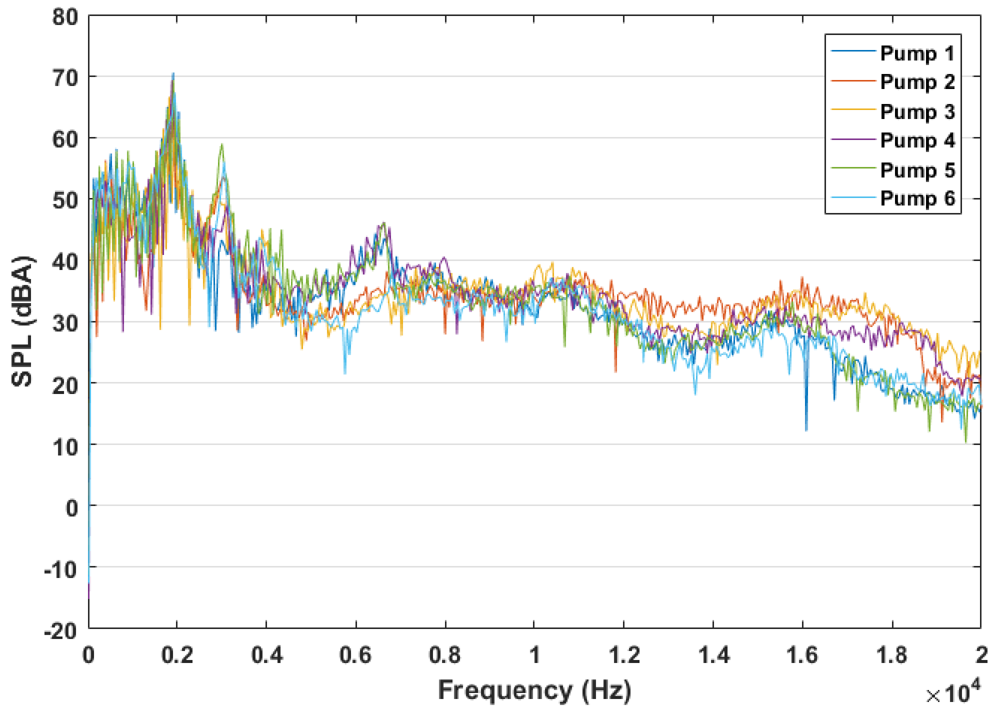

Figure 17: All spec pump comparison under ambient operation speed not controlled

Figure 17 above is a display of 6 spec pumps that are operating without back pressure (ambient condition) and without speed control. The pump motor operated between 63.63 Hz and 65.53 Hz. Of all the spec pump acoustic testing pumps operating in ambient conditions without speed control resulted in the highest magnitude pressure waves with the greatest acoustic peak at 2000 Hz topping out just above 70 dBA. The 2000 Hz spike was also seen in the first ambient test displayed in Figure 16. The presence of a secondary spike at approximately 3000 Hz is dissimilar to Figure 16. Harmonics were dismissed as the cause due to the spike location not occurring at a multiple of 2000 Hz. The spike was at a different frequency from the 12 psi back pressure spec tests and reached a maximum magnitude between 58 and 69 Hz.

Figure 16 and Figure 17 display very similar acoustic signatures with the rise to a peak at 2000 Hz followed by a decline of acoustic pressure at higher frequencies. The noise floor of Figure 17 is slightly higher than that of the ambient test with speed control. The lowest magnitude pressure waves of the 6 pump test were centered close to 20 dBA and occur between 18000 Hz and 20000 Hz.

Defect Orientation Investigation

In the pump under test the diaphragms were located on opposing sides of the motor. This opposite side arrangement was implemented in order to help balance the eccentric rotation during pump operation. Part of the study sought to classify the differences in pump acoustics based on the side that the defect was introduced. If a defect introduced to a specific side were to produce an acoustic signature of lesser magnitude, that side would be used as the diagnostic threshold. By using the acoustic signature with the least pronounced differences, the diagnostic tool would pick up the defect independent of side orientation.

In order to determine if a particular side of a pump produced a different acoustic signature two trials were captured for every condition that each pump was tested under. The trials were identical except for the defect orientation on opposite sides of the pump. Because no noticeable differences were recorded during the defect orientation investigation the presented data has been limited to one envelope plot that displays normal results for pumps operating under 12 psi back pressure with speed held at 45 Hz.

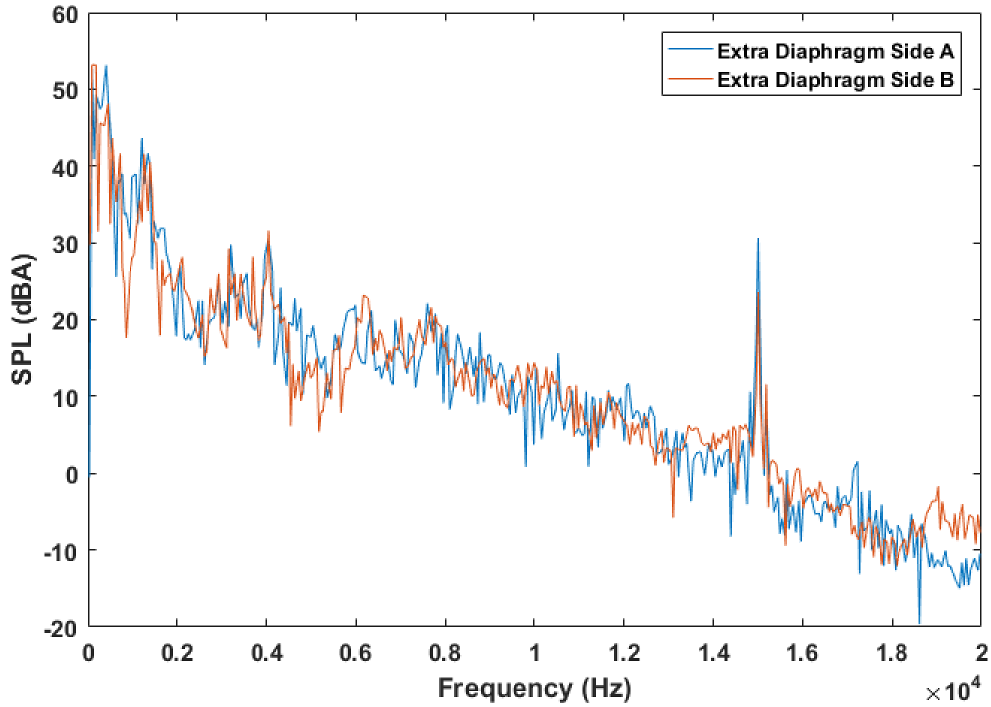

Figure 18: Pump 5 side A vs B comparison for ED under 12psi back pressure controlled

Figure 18 displays Pump 4's acoustic signature with the extra introduced diaphragm on opposing sides of the pump. The two acoustic signature envelope plots are very similar in shape. There is no noticeable difference in the magnitudes of the envelope plot based on the side of the pump that the defect resides. Similar results were recorded for all other pumps under all other conditions (12psi speed not controlled, ambient speed controlled, and ambient speed not controlled).

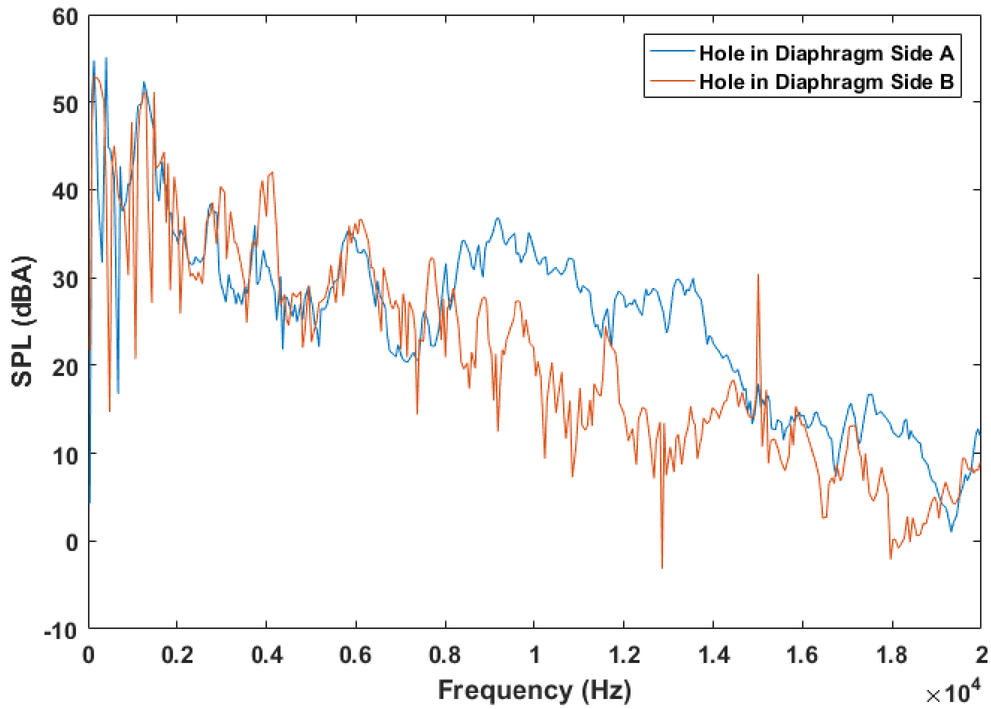

Figure 19: Pump 4 side A vs B comparison for hole in diaphragm under 12 psi back pressure controlled

Figure 19 contains envelope plots for Pump 4 with a hole in one diaphragm while operating under 12 psi back pressure with the speed controlled at 45 Hz. The blue envelope was resultant of a pump with the damaged diaphragm fixed to side A of the pump. The red envelope was produced by a pump with the damaged diaphragm on side B. The two plots are noticeably different, however, running multiple data sets proved no correlation to side A or side B. It was discovered that there are two characteristic plot shapes for hole in diaphragm defects. These were named trend 1 and trend 2; this topic is discussed in detail later in this section.

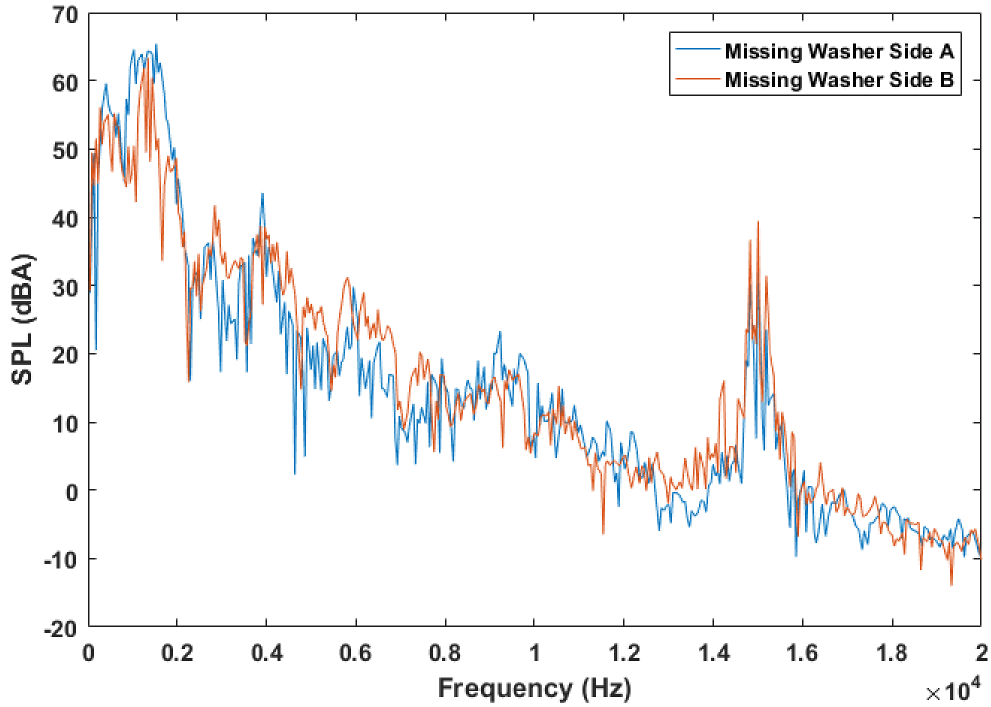

Figure 20: Pump 3 side A vs B comparison for MW under 12psi back pressure controlled

Figure 20 is a plot of Pump 3 with a washer omitted from one side of the pump. The test was also recorded while the pump was operating at 45 HZ rotational speed under 12 psi back pressure. There was no noticeable difference in the acoustic envelope of pump 3 with the defect on opposite sides of the pump. All other testing conditions exhibited similar results, in that the defect caused a similar signature despite the orientation on specific sides of the pump.

Hole in Diaphragm Angular Investigation

A study was performed to assess the effect of the hole in diaphragm placement. The angular position of the diaphragm rip was varied according to Figure 21 in order to pinpoint the position with the weakest acoustic change. As in the defect orientation study, the position with the weakest acoustic signature was implemented during testing to ensure all holes in the diaphragm are detectable by the finished prototype.

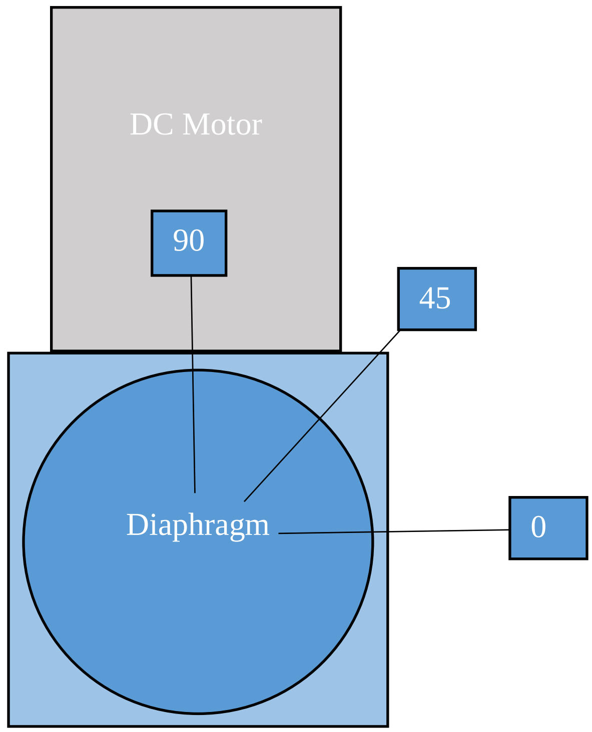

Figure 21: Hole in diaphragm angular position

An example hole in the diaphragm that could be introduced during the diaphragm manufacturing process is displayed in Figure 22

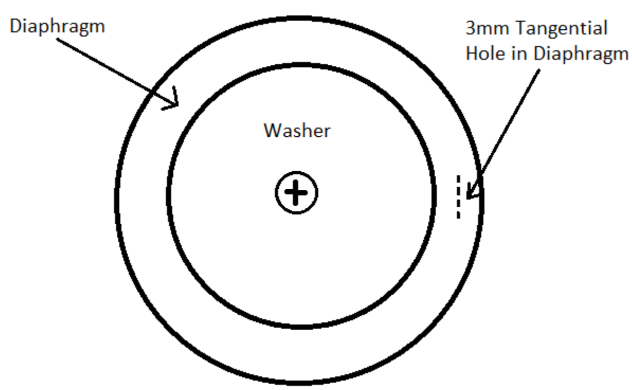

Figure 22: Example hole in the diaphragm

The hole in the diaphragm displayed in Figure 22 is oriented at 0 degrees according to Figure 21. The results of the hole in the diaphragm angular placement test are found in Figure 23 below.

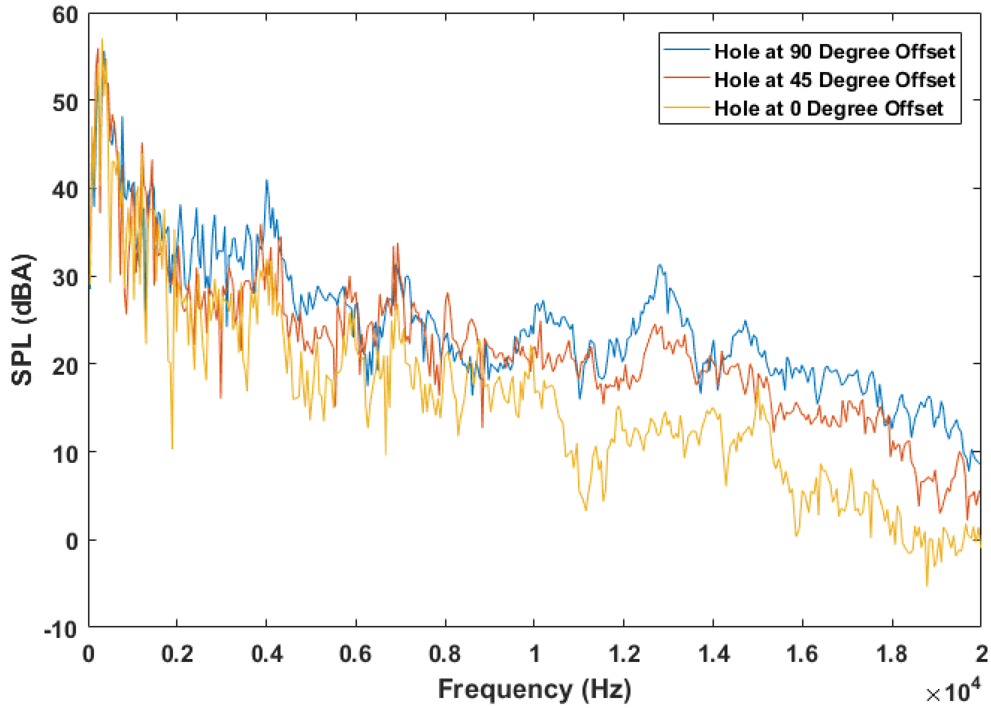

Figure 23: Hole in diaphragm angular position investigation for pump 1

The trends of the three plots are very similar. The lower pitched acoustic energy 0 to 2000 Hz display almost identical results, while the higher frequency content, 2000 Hz to 20 kHz, display variability. The higher range (600 to 20,000 Hz) is attributed to the aeroacoustical interactions within the air stream. Altering the hole placement on the diaphragm altered the air flow interactions of the pump, possibly causing the variation in the higher frequency ranges. While differences were expected in the flow stream, the mechanical elements of the pump were moving at the same rate. The weakest acoustic signature was when the hole was located at zero degrees and is at a right angle with the

DC motor. This position was selected for the remainder of the hole in the diaphragm testing.

Acoustic Defect Results

Extra Diaphragm Comparison

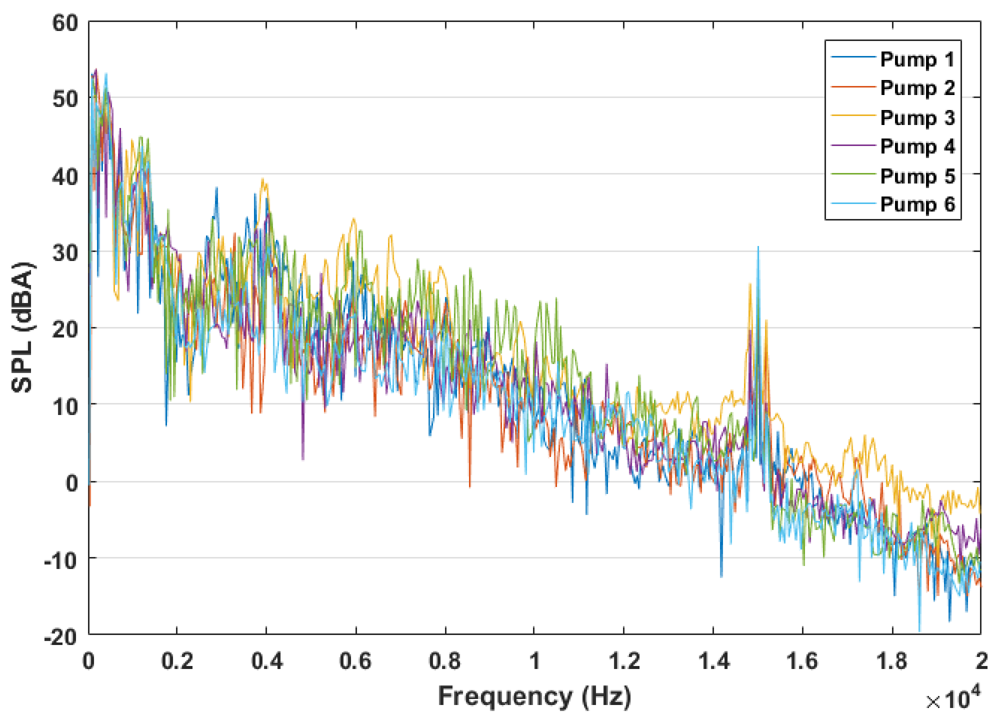

Figure 24: 6 pump envelope comparison of extra diaphragms 12 psi controlled

Figure 24 displays all 6 pumps with an introduced defect of an additional diaphragm under 12psi back pressure with a motor rotational speed of 45 Hz. The results of an additional diaphragm placed on a piston head were very similar to the spec pump results under the same operating conditions. The majority of the acoustic energy was found in the lower range with a maximum pressure magnitude of 54 dBA. The secondary spike that was found in the spec 12 psi testing was also produced in the 12 psi extra diaphragm testing. The secondary spike can be reviewed in Figure 14 and Figure 15.

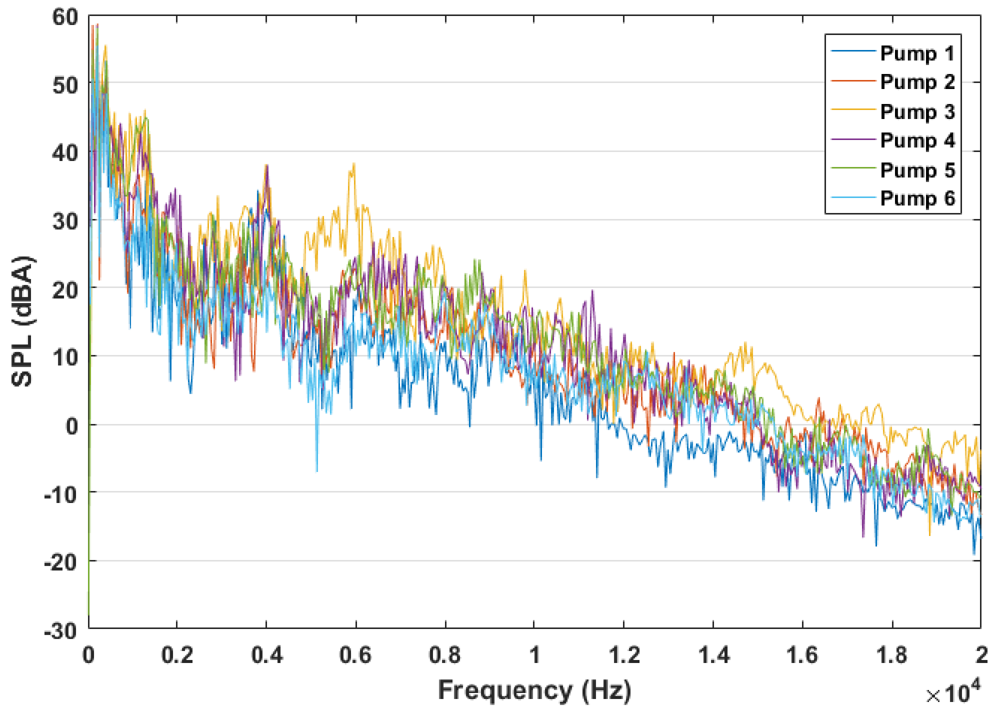

Figure 25: 6 pump envelope comparison of extra diaphragms 12 psi not controlled

Figure 25 shows the envelope plot of the 6 extra diaphragm pumps operating under 12 psi back pressure without any motor control. The motor driving the pump pistons only achieved a rotational velocity range of 49.15 Hz to 52.37 Hz. Similar to Spec pump testing, the 12 psi back pressure plots for the extra diaphragm testing display very similar acoustics. A noted difference between the two is that Figure 25 lacks the noise spike at 15 kHz that is visible in Figure 24 which was attributed to lack of motor control. Another parallel that was drawn between the spec pump testing and the extra diaphragm testing was that the uncontrolled speed tests produced slightly higher acoustics in the lower frequency range below 600 Hz than testing where the motor speed was held at 45 Hz.

Centered at 4000Hz is a visible spike that is similar to other 12 psi back pressure testing. The spike is visible in the spec 12 psi testing as well as in Figure 24. A slightly uncharacteristic behavior is noted in the pump 3 envelope (yellow plot) between 4000 and 6000 Hz. The rise in acoustic magnitudes between this zone was mainly attributed to the pump operating slightly louder than other similar pumps and was prominent in the spec pump testing.

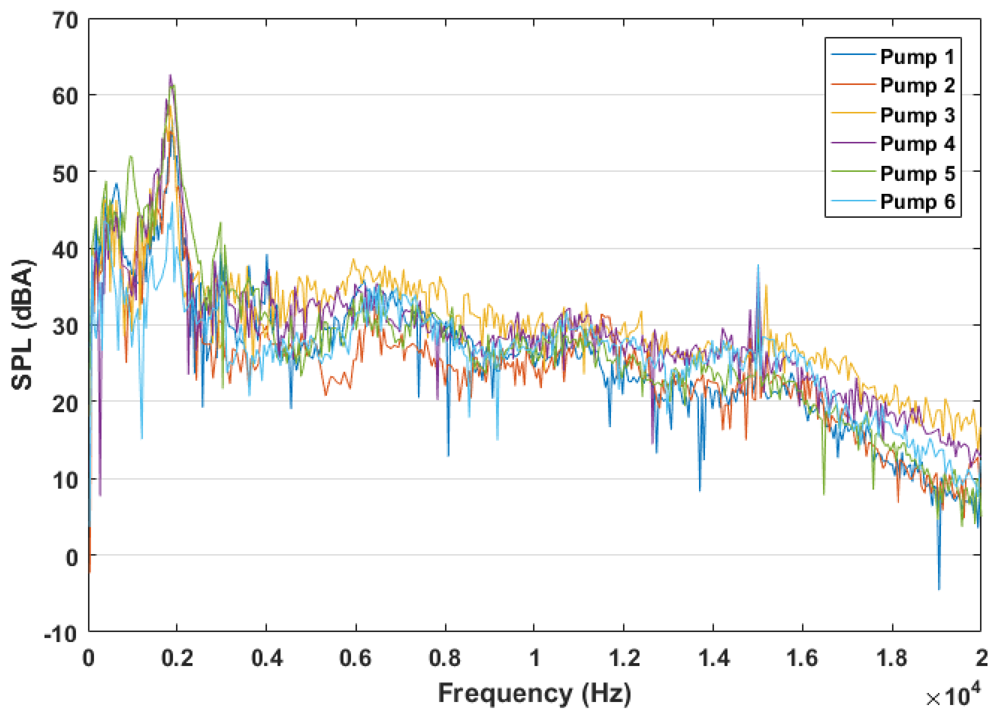

Figure 26: 6 pump envelope comparison of extra diaphragms ambient controlled

Figure 26 is the envelope plot of 6 pumps with an extra diaphragm on one piston head, operating in ambient conditions, with the speed held at 45 Hz. The response between 20 and 2000 Hz is similar to the ambient controlled spec pump testing in that the plot displays a rise to a maximum peak at 2000 Hz. There is no prominent secondary spike that is visible in Figure 26, which is also consistent with the spec pump tests under the same conditions.

Pump 6 (in blue) produced a slightly lower acoustic signature than the other pumps in the ambient speed controlled trial. This quiet behavior was not visible or audible in other testing. The blue plot reached a maximum of approximately 46 dBA at 2000 Hz while other pumps topped out above 60 dBA. The high end of the acoustic range displayed very similar results to the spec testing under consistent operation parameters. The envelope between 18 kHz to 20 kHz was centered on 12 dBA.

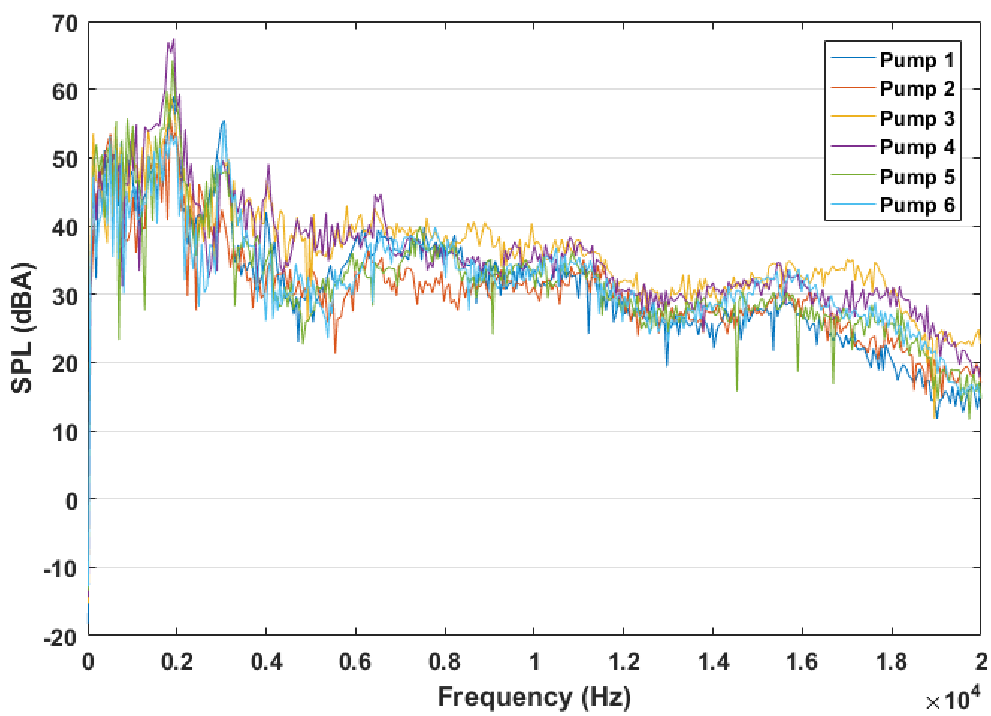

Figure 27: 6 pump envelope comparison of extra diaphragms ambient not controlled

Figure 27 is a display of 6 pumps with extra diaphragms added to one side operating without back pressure or speed control. As with all ambient testing, a noticeable spike was produced at approximately 2000 Hz. Pump 6 did not display the same quiet behavior that was observed in Figure 26. The secondary acoustic peak that was visible in the spec ambient not controlled test appears in Figure 27 which suggests that the secondary spike is common under the testing conditions. The spike is located right at 3000 Hz and reaches a magnitude between 50 and 55 dBA. The rotational speed of the pumps operating under ambient conditions varied from 61.71 Hz to 64.31 Hz.

Hole in Diaphragm Comparison

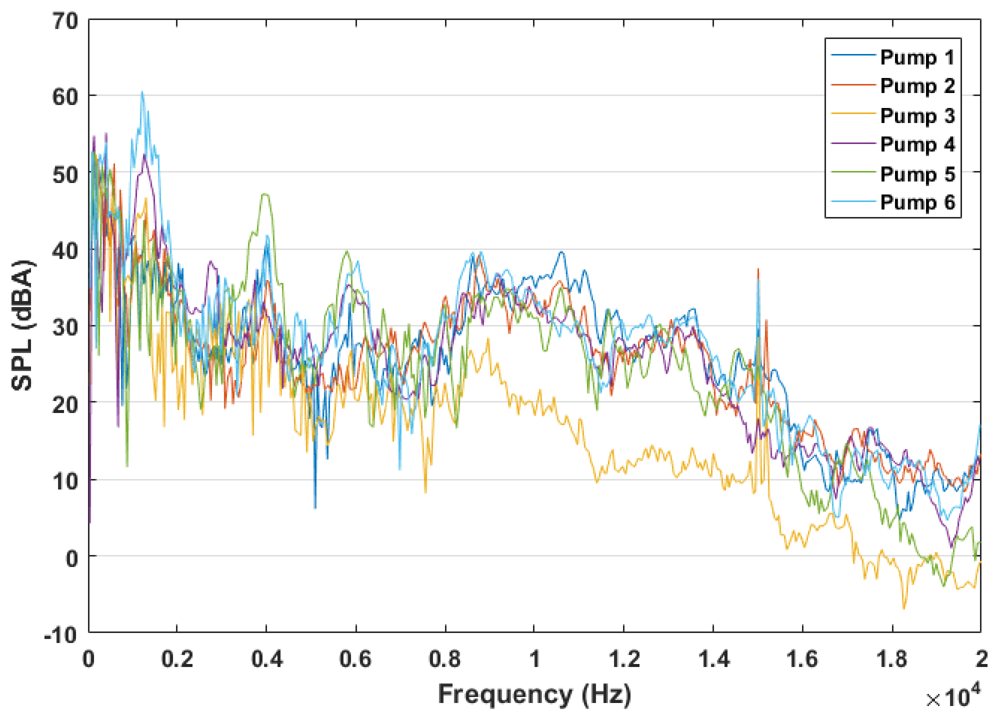

Figure 28: 6 pump envelope comparison of hole in diaphragms 12 psi controlled

Figure 28 is a plot of all 6 pumps with an introduced defect of a hole in the diaphragm under 12psi back pressure with a motor rotational speed of 45 Hz. To reiterate the holes in the diaphragm were all introduced at the quietest angular position of 0 degrees (see Figure 21). Two distinct trends were noted during the extent of the hole in the diaphragm testing: cases where higher acoustical energy appeared in the 8000 to

20000 Hz range, and cases where this acoustic energy was less pronounced. Pump 3 (yellow) did not display the increase in acoustic energy over this range while all other tested pumps did exhibit increased energy.

Pumps with holes in the diaphragm produced similar frequency content trends to spec pumps over the range of 20 to 8000 Hz. The secondary spike is visible at 4000 Hz in Figure 28 for all tests with a fluctuating magnitude. Dissimilar to spec tests under the same conditions, was the magnification of an acoustic frequency peak between 1000 and 2000 Hz. This peak, while not prominent in the spec pump testing, was of greatest magnitude for the 12 psi controlled hole in the diaphragm testing for pump 4 and pump 6.

The two distinct trends that are apparent in the hole in the diaphragm testing with 12 psi back pressure at a controlled speed are likely due to the differences in the diaphragm holes. If one hole was slightly more covered by the diaphragm washer than others the pump may have been less effected by the defect. If the hole in the diaphragm were completely exposed the pump would be more effected, leading to pressure loss or turbulence introduced into the flow path. A hole in diaphragm changing the mechanical load on the pump can lead to serious differences in operating condition, thus leading to a large amount of variability in the acoustics.

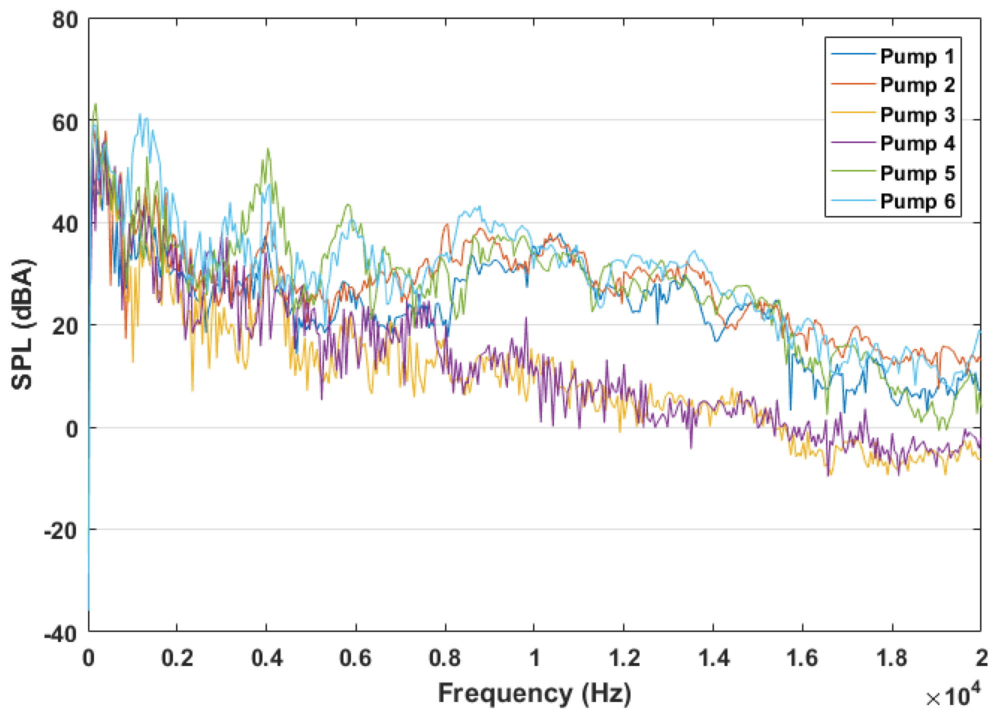

Figure 29: 6 pump envelope comparison of hole in diaphragms 12 psi not controlled

Figure 29 displays the envelope plot of the 6 pumps with an introduced hole in the diaphragm operating under 12 psi back pressure without motor control. The DC motor operated with in the rotational velocity range of 53.18 Hz to 57.72 Hz. Similar to Figure 28, two distinct trends were noted in the 6 pumps tested: pumps with elevated acoustic magnitudes between 8000 and 20000 Hz and pumps that had less energy over this frequency range. Pump 3 and Pump 4 in Figure 29 produced far less acoustical energy over this range than the other pumps tested. It should be noted that acoustic signatures of the same trend are consistent in shape and magnitude. Pumps exhibiting the higher acoustic trend produced magnitudes in the frequency range of 18 kHz to 20 kHz centered around 10 dBA; pumps exhibiting the lower acoustic trend produced magnitudes centered around -5 dBA.

The prominent peak that is noted in Figure 28 at a frequency between 1000 and 2000 Hz was also produced by pump 6 in the 12 psi test without speed control. The secondary peak at 4000 Hz is visible in all pump trials of Figure 29, which is consistent with the majority of all 12 psi testing.

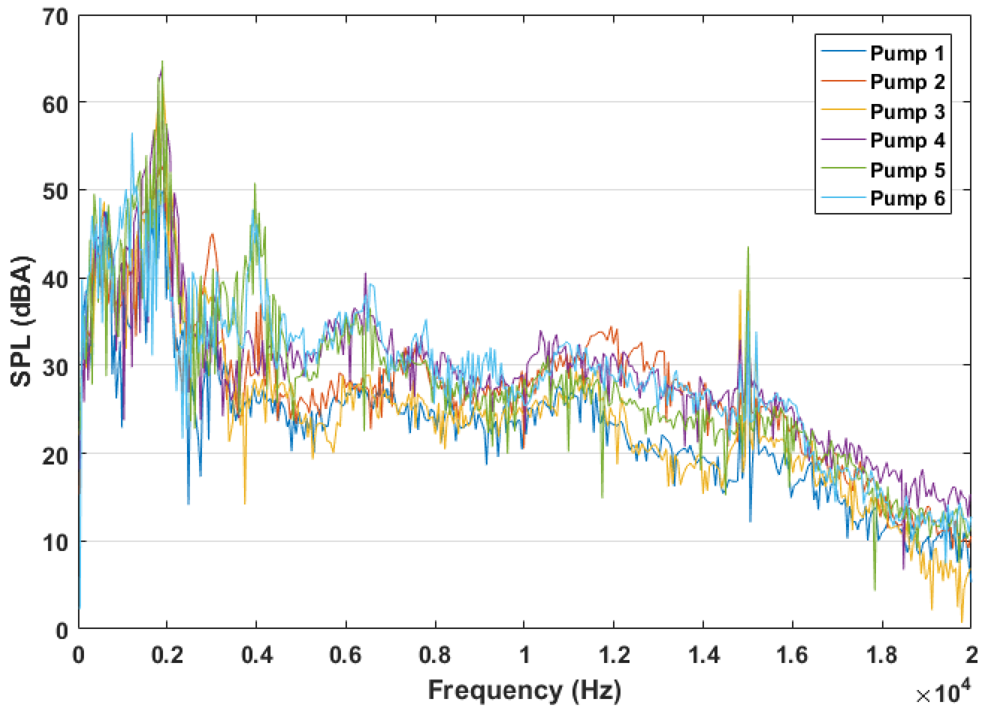

Figure 30: 6 pump envelope comparison of hole in diaphragms ambient controlled

Figure 30 is a display of the envelope plots of the 6 pumps with a hole introduced into the diaphragm. The pumps were operating under ambient conditions with the speed of the motor held at 45 Hz. Similar to spec testing the pump acoustics under ambient conditions produced a higher acoustic magnitude than similar pumps under back pressure. The two distinct acoustic behaviors (trend one and two) that were visible in Figure 29 and Figure 28 are not visible under ambient conditions. The lack of the distinct trends in the ambient graph may indicate that the dividing factor between trend 1 and trend 2 for 12 psi testing was variable pressure. The lack of back pressure on the ambient pump may have resulted in the consistent envelope shape observed in Figure 30.

The hole in the diaphragm testing displays the 2000 Hz spike that is characteristic of ambient pump operation. Another notable spike is produced by Pump 5 and Pump 6 around 4000 Hz. Though this was not produced by the other hole in the diaphragm pumps under the same conditions, the 4000 Hz spike was commonly noted in 12 psi back pressure tests.

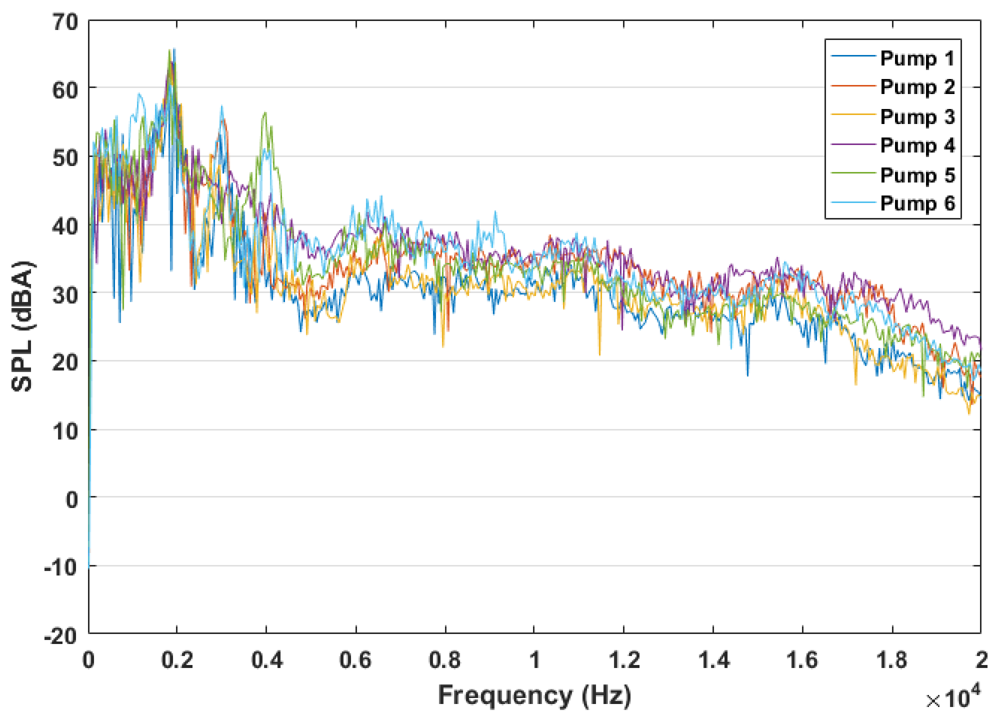

Figure 31: 6 pump envelope comparison of hole in diaphragms ambient not controlled

Figure 31 displays the envelope plots of 6 pumps with holes in one diaphragm that are operating without back pressure and without speed control. The rotational speed varied from 63.76 Hz to 66.44 Hz. The maximum acoustic magnitude of the plots was around 2000 Hz with magnitudes well above 60 dBA. The high end of the frequency spectrum between 18 kHz and 20 kHz contains acoustic envelopes centered on 20 dBA, which was similar to spec pumps operating under similar conditions. The peak that is observed in the spec pump ambient speed not controlled testing around 3000 Hz is also prevalent in Figure 31. Pump 4 and Pump 5 produced a tertiary peak centered at 4000 Hz though this characteristic was not consistent with the other pumps.

Missing Washer Comparison

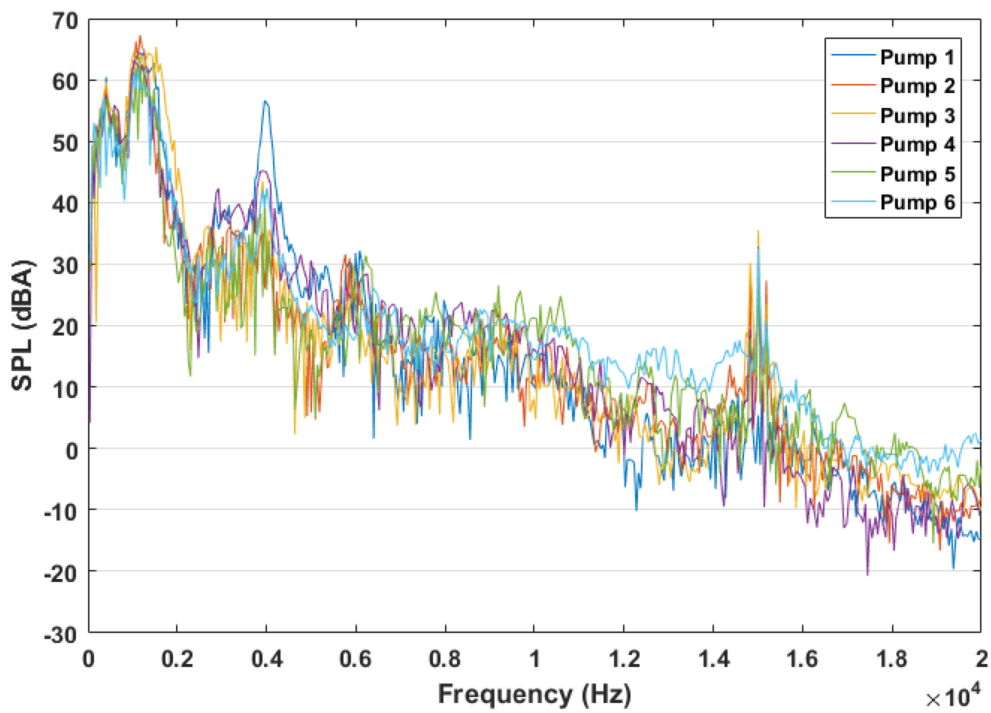

Figure 32: 6 pump envelope comparison of missing washers 12 psi controlled

Figure 32 is an envelope plot of all 6 pumps with an introduced defect of a missing washer under 12psi back pressure with a motor rotational speed of 45 Hz. The missing washer tests produced a very distinguishable acoustic spike around 1200 Hz that is not characteristic of 12 psi back pressure testing but is visible in two pumps in Figure 28. A characteristic that is common with other pump testing is the acoustic pressure spike at 4000 Hz. The spike is consistent with all 6 pumps of Figure 32. Pump 1, however, produced acoustic pressure waves that were of a far greater magnitude than others. A spike that was consistent of all missing washer pumps was produced at 300 Hz.

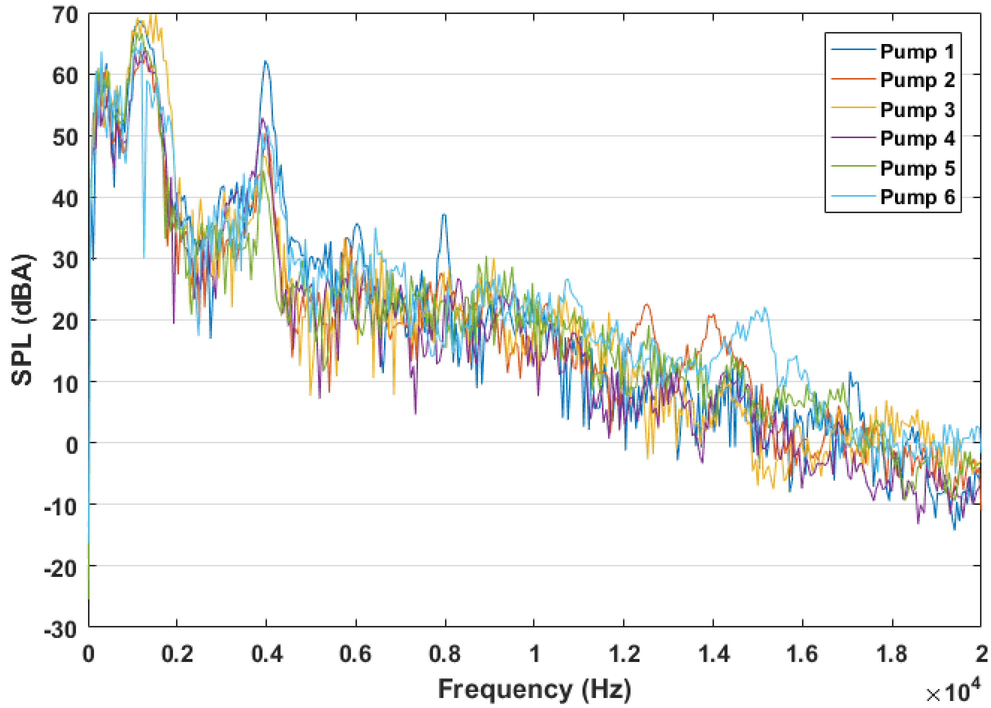

Figure 33: 6 pump envelope comparison of missing washers 12 psi not controlled

Figure 33 displays the envelope plot of the 6 pumps operating without a washer on one diaphragm under 12 psi back pressure without any motor control. The shape of the envelope plots for 12psi back pressure without speed control is very similar to those found in Figure 32. Rotational speed of the pump motor operated over a vast range of 56.88 Hz to 64.31 Hz. The same three spikes are produced: 300, 1200 and 4000 Hz. Again, the most prominent spike was centered at 1200 Hz. The highest magnitude of the 6 pumps was just under 70 dBA, slightly higher than the controlled speed trials. Similar to in Figure 32, pump 1 produced pressure waves of far greater magnitude at the 4000 Hz frequency spike.

Pump 6 displayed uncharacteristic behavior centered around 1200 Hz. While most pump acoustic envelopes were above 60 dBA, pump 6's envelope dipped down to 30 dBA. This effect was due to the find peaks MATLAB function recognizing a low peak between the main acoustic spikes that are propagating as multiples of the fundamental. Separating the acoustic peaks by an interval of 45 generated a good representation of the majority of acoustic energy. When the pump motor's rotational speed was not controlled the major acoustic peaks were not spaced evenly at 45 Hz. The lower characteristic of the acoustic envelope of pump 6 in Figure 33 is a low peak that was highlighted between major peaks.

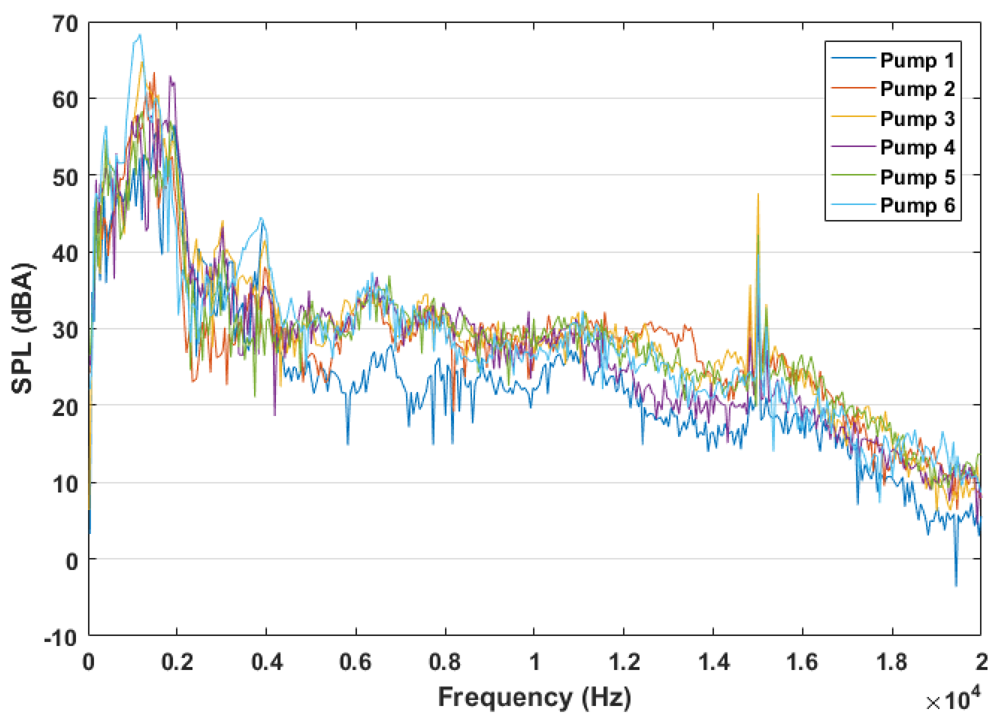

Figure 34: 6 pump envelope comparison of missing washers ambient controlled

Figure 34 is a 6 pump envelope plot where the piston washer on top of the diaphragm was omitted from one side of the pump. The plot is while the pumps were operating at 45 Hz under ambient conditions. The majority of the acoustic energy was propagating at frequencies between 1000 and 2000 Hz, with the highest magnitude at approximately 68 dBA. While the frequency with the greatest acoustic peaks in Figure 32 and Figure 33 are very constant, Figure 34 does not display the same consistency. Though a large amount of acoustic energy is located at a similar range, the peaks do not appear to be centered at a specific frequency. The greatest acoustic envelope peak was produced by pump 6, and was propagating at around 1200 Hz. Other similar significant peaks were spread out and located at frequencies up to 2000 Hz (pump 4).

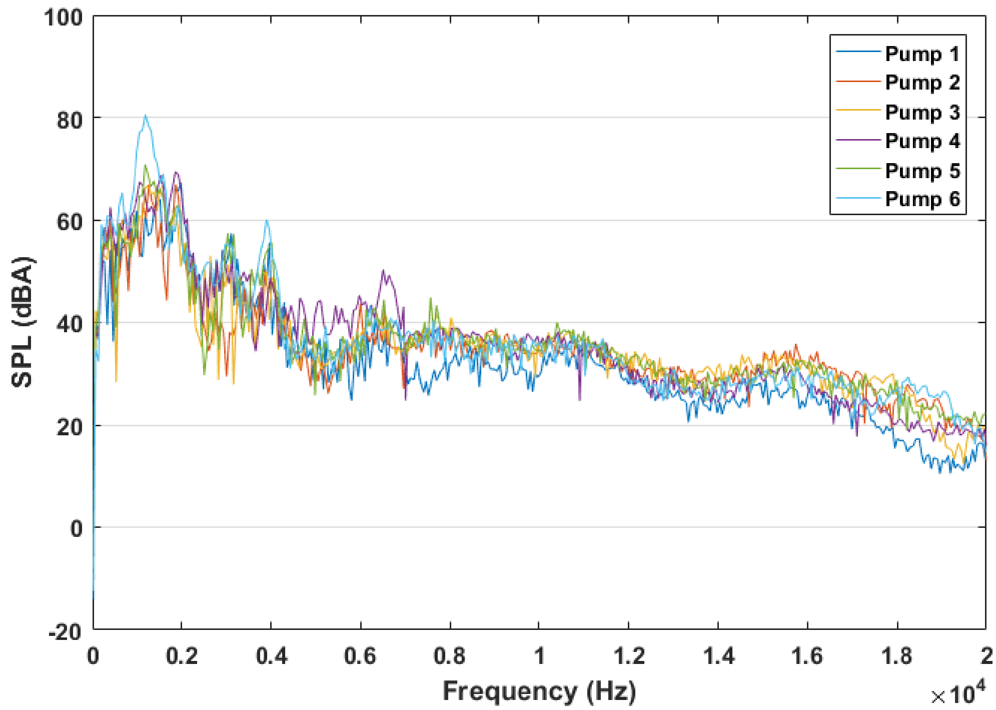

Figure 35: 6 pump envelope comparison of missing washers ambient not controlled

Figure 35 shows the acoustic envelope of 6 pumps that were operating without back pressure and without speed control that all have a missing washer on one piston. The rotational speed of the pump motor was variable within the range of 65.81 Hz to 67.56 Hz. The greatest acoustic pressure magnitude of all acoustic testing was achieved by pump 6 during the ambient no speed control testing with a peak magnitude just over 80 dBA. It was observed that pump 6 produced the higher magnitude acoustics than the other pumps for the ambient missing washer tests; this behavior was observed for pump 6 in other defect testing, and was investigated further.

The envelopes of the 6 pumps in Figure 35 show a rise in acoustic pressure from 1000 and 2000 Hz, though no consistent peak location is present. A spike at 4000 Hz was common which is characteristic of ambient testing without speed control independent of pump status. Another significant pressure spike was located at 3000 Hz though pump 2 and 3 did not appear to have significantly elevated acoustic pressure at this frequency. Discrepancies from the normal acoustics of a missing washer pump include the large magnitude of pump 6 around 1000 Hz and the increase of pump 4’s acoustics at 6500 Hz.

DISCUSSION

After extensive testing of all defective and spec pumps under ambient and back pressure conditions, it was concluded that the pumps operating under ambient conditions display very few acoustic differences. Defective pumps produced very similar acoustics to spec pumps while pumping air without back pressure, therefore it was determined that back pressure is required for acoustic quality inspection of the pump under test. Moving forward, analysis and the development of the prototype diagnostic procedure focused on tests of pumps operating against back pressure. The figures of defective pumps plotted against spec pumps in ambient conditions are located in the appendix.

Extra Diaphragm to Spec Comparison

To display a clear picture of the acoustic differences between the defective pumps and the spec pumps two typical envelope plots are displayed in a single figure for each of the 12 psi operating conditions. The envelope plots that were chosen are very consistent with the normal behavior of the tested pumps. The plots were chosen to represent the acoustics of the six pumps’ behavior while not over-crowding the graphic.

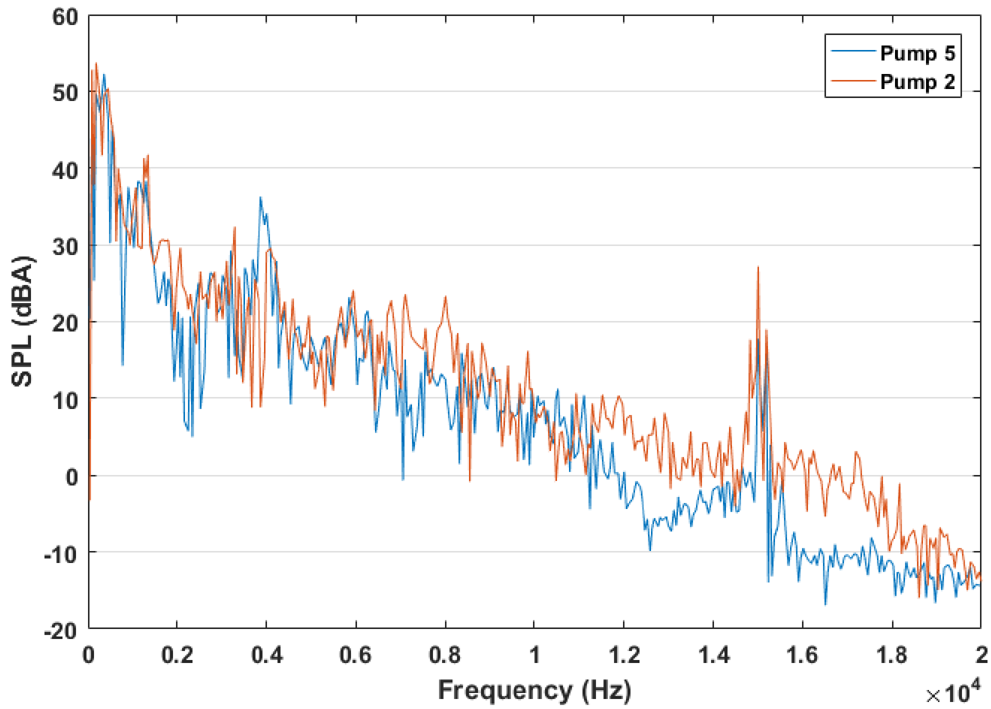

Figure 36: Envelope plot of extra diaphragm pump compared to normal pump 12psi controlled

Figure 36 is a graphic of a spec pump (blue) and an extra diaphragm pump (red) operating at 45 rotations per second under 12 psi back pressure. Both pumps produced very similar acoustics. The envelope plots contain the maximum acoustic magnitude below 1000 Hz and both display a secondary spike at 4000 Hz. The secondary spike produced by the extra diaphragm pump was of slightly lesser magnitude than the spec pump signature, though this was not always consistent for every trial. The extra diaphragm acoustics were of slightly higher magnitude in the range of 11 kHz to 20 kHz. The increase in the acoustic energy over this range was not significant, because the 6 spec pumps' acoustic signatures over the 11 - 20 kHz range for the 12 psi back pressure testing displayed similar variability. The acoustic envelopes displayed a variability sometimes diverging by up to +/- 10 dBA.

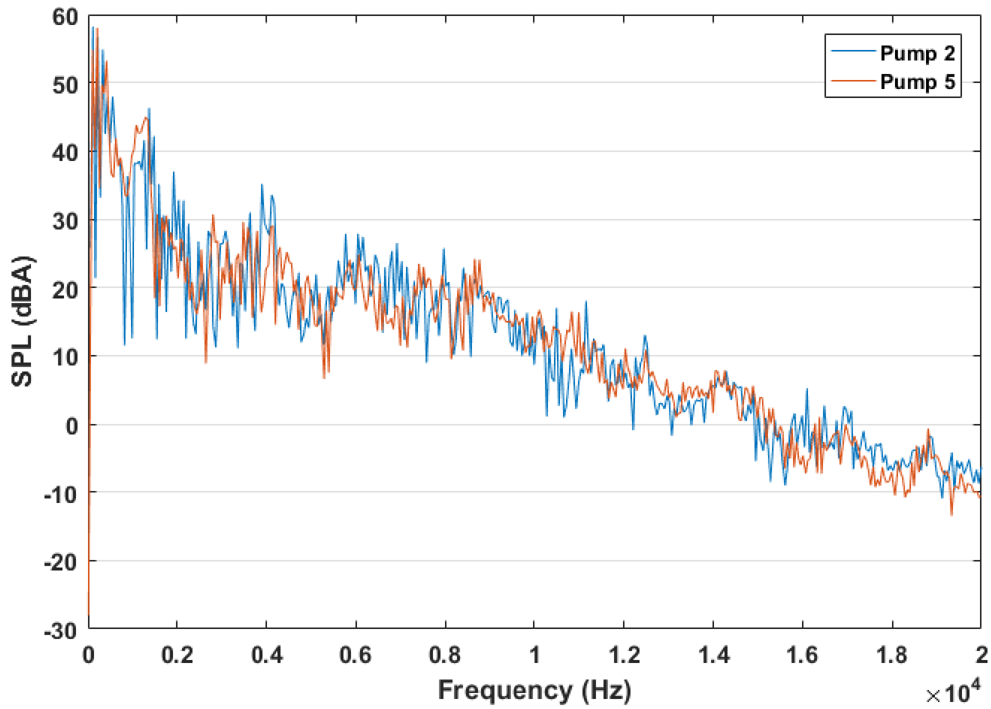

Figure 37: Envelope plot of extra diaphragm pump compared to normal pump 12psi not controlled

Figure 37 is a display of a spec pump and a pump with an extra diaphragm that were operating at 12 psi without speed control. Note the absence of the 15 kHz spike. The two envelope plots are very similar in magnitude and shape. Both pumps produced their highest magnitudes below 1000 Hz and both exhibited a secondary acoustic peak around 4000 Hz. The majority of the extra diaphragm testing that occurred resulted in acoustic signatures that were indistinguishable from spec acoustic signatures.

Hole in Diaphragm to Spec Comparison

To show clear distinction between the defective pumps and the spec pumps envelope plots are displayed in a single figure for each of the 12 psi operating conditions. The envelope plots that were chosen highlight specific trends that were consistently observed during pump testing. The hole in the diaphragm testing resulted in two distinct trends. Both trends were plotted and compared against a spec pump operating under identical conditions.

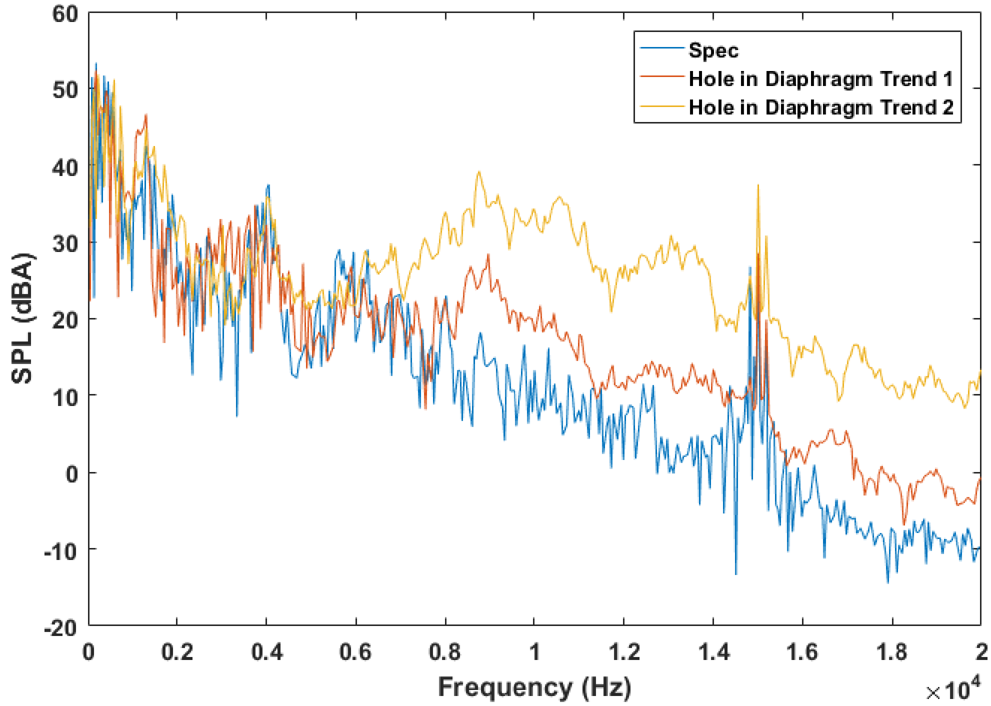

Figure 38: Envelope plot of hole in diaphragm pump compared to normal pump 12psi controlled

Figure 38 is a graphic containing the two distinct behaviors of pumps with holes in the diaphragm compared to a spec pump. All pumps in Figure 38 were operating under 12 psi back pressure and were running at a speed of 45 Hz. The pump acoustics are very similar in the mechanical range from 20 to 600 Hz. The signatures display uniformity up to approximately 7000 Hz where differences are noted.

Both trend 1 and trend 2 of the hole in the diaphragm pumps produced increased acoustics over 7000 Hz. This trend was less apparent in the pump producing trend 1 acoustics when compared to the trend 2 pump. Figure 14 clearly displays that a spec pump under the same operating conditions would vary by up to 10 dBA. The variable nature of the spec pump acoustics limits the value of trend 1's increase in acoustic energy. The increase in acoustic energy of trend 1 acoustic signature over the 7 – 20 kHz range was within the spec pump +/- 10dBA range.

The significant increase in acoustic energy of trend 2 leads to a clear conclusion that the pump contained a defect. The acoustics of trend 1 were slightly more challenging to distinguish from a spec pump. Occasionally a spec pump acoustic signature in the 7000 Hz -20000 Hz range could produce acoustics that match trend 1 in magnitude making false diagnostics possible for a healthy pump. With such similar acoustic signatures, possibility also exists that a pump with a hole in the diaphragm exhibiting trend 1 behavior could be passed by the quality inspection device.

In order to decrease the possibility of false diagnostics a more detailed look at the full acoustic signature of hole in the diaphragm pumps was required.

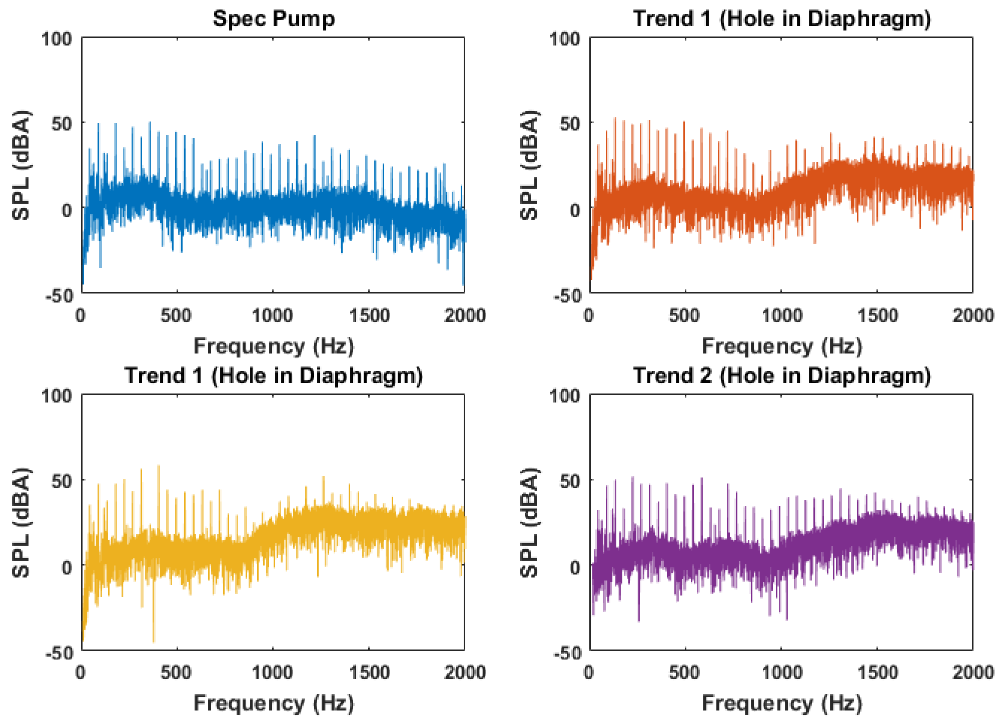

Figure 39: Three hole in diaphragm FFT plots compared to a spec FFT plot 12 psi controlled

Figure 39 displays 4 plots of raw FFT samples plotted from 0 to 2000 Hz. The blue plot is of a spec pump operating at 45 Hz with 12 psi back pressure. The remaining plots are of acoustic signatures of pumps with holes in their diaphragms operating under the same conditions. The orange and purple plots are of pumps with trend 1 behavior and the gold plot is a pump with trend 2 behavior.

The majority of the acoustic data was clustered at lower magnitudes than the large spikes that propagated as multiples of the rotational frequency. The acoustic data cluster of the spec plot remained relatively flat across the 2000 Hz window, while the pumps with holes in their diaphragms produced an elevated characteristic starting at 1000 Hz. Though not visible while viewing the envelope plot, this increase in the "acoustic floor" is a telltale sign of a punctured diaphragm.

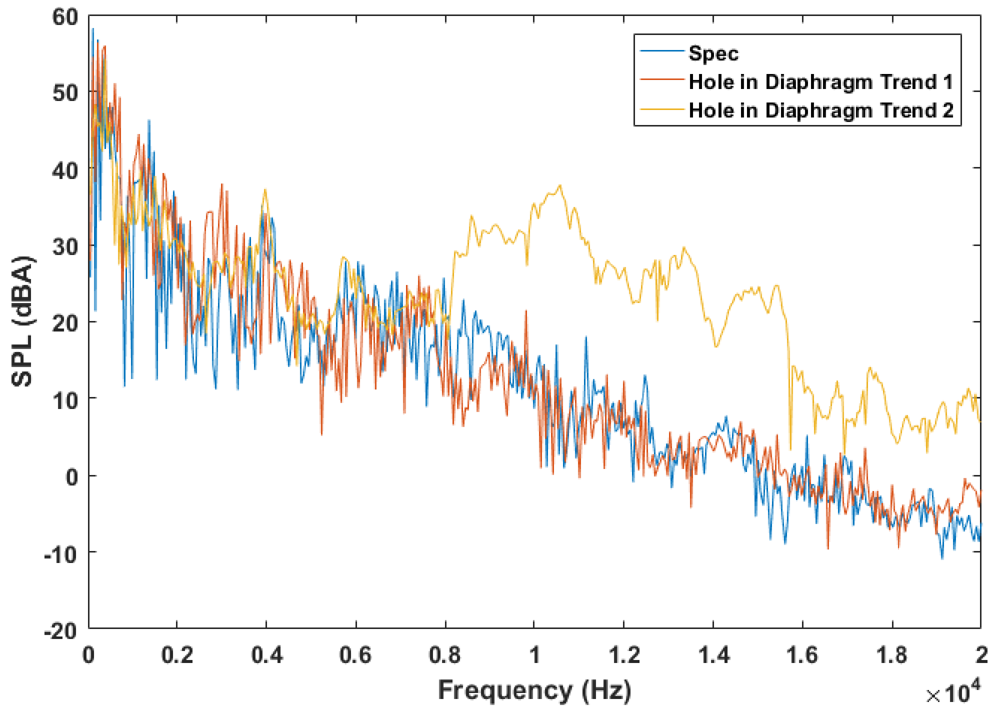

Figure 40: Envelope plot of hole in diaphragm pump compared to normal pump 12psi not controlled

Figure 40 displays the significant trends of pumps with holes in their diaphragm compared to a spec pump (blue). The pumps were operating under 12 psi back pressure without speed control. Figure 40 more clearly portrays why a closer look at the full pump acoustic signature for hole in the diaphragm pumps must be investigated. The pump that exhibited trend 1 acoustics (less acoustic energy is produced over the higher frequency band) was indistinguishable from the spec pump acoustic envelope.

While it was easy to conclude that there was a problem with a pump producing trend 2 acoustics (yellow plot), trend 1 proved difficult to differentiate from a spec pump, even though it contained a known defect. In order to distinguish a hole in diaphragm pumps with trend 1 acoustics from spec pump acoustic the full acoustic signatures were analyzed.

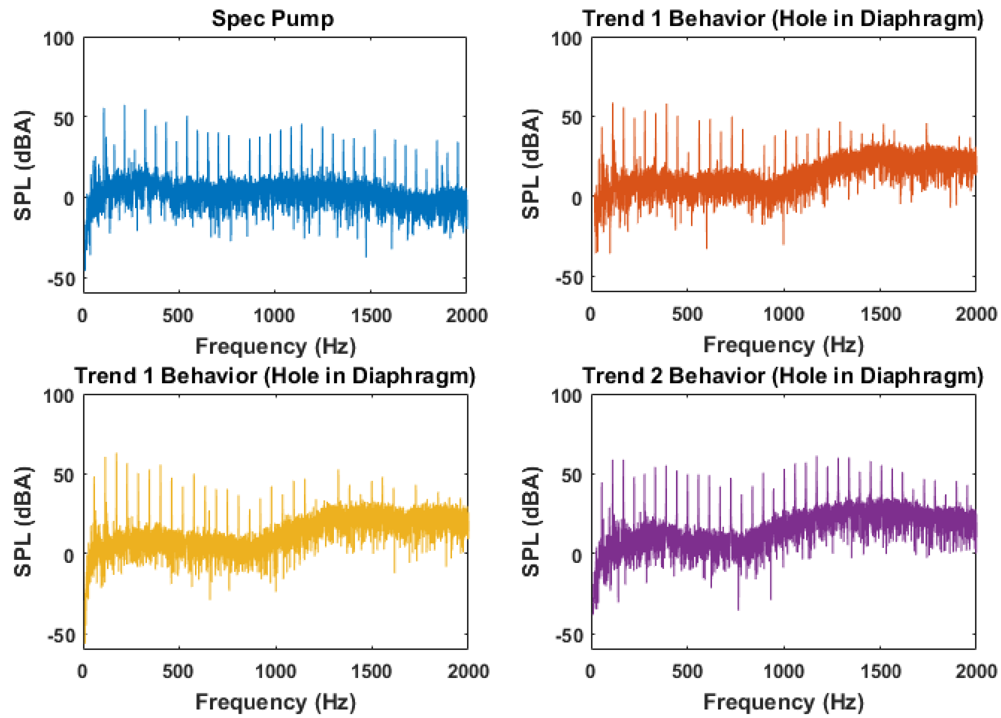

Figure 41: Three hole in diaphragm FFT plots compared to a spec FFT plot 12 psi not controlled

Figure 41 is a collection of FFT plots from 3 pumps with holes in one diaphragm and a spec pump all operating under 12 psi back pressure without motor control. The same acoustic floor elevation that was noted in Figure 39 is visible in the plots three plots that of diaphragms with holes (purple, gold and red). The orange and yellow plots were acoustics of pumps that exhibit trend 1 behavior while the purple plot was a signature from a pump producing the more common trend 2 acoustics. All of the hole in the diaphragm pumps produced an elevated acoustic floor from 1000 Hz to 2000 Hz, while the spec pump acoustic floor remained relatively constant.

Missing Washer to Spec Comparison

In order to show clear acoustical differences between pumps with a missing washer and spec pumps, two pumps envelopes were plotted in a single figure for each of the 12 psi operating conditions. The envelope plots for the missing washer tests were chosen to represent the general trend of all of the pump trials. Not every missing washer trial is plotted against a spec trial under the same conditions in order to highlight acoustic differences.

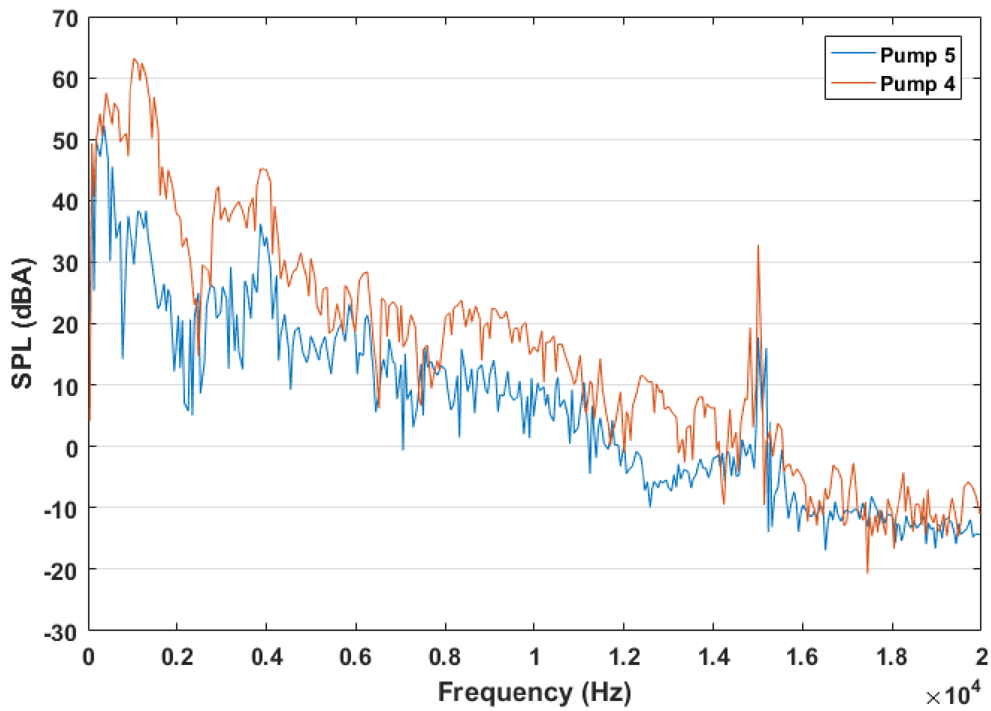

Figure 42: Envelope plot of missing washer pump compared to normal pump 12psi controlled

Figure 42 displays a spec pump in blue and a pump with a missing washer in red. The pumps were operating with 12 psi back pressure and a constant speed of 45 Hz. The majority of the acoustical difference occurred in the low frequency range below 2000 Hz. The pump with a missing washer produced much greater acoustic output in the range of 20 to 2000 Hz than the spec pump.

The large increase in the acoustic energy between 1000 and 2000 Hz was a telltale sign that a washer is missing. The consistency of this increase can be viewed in Figure 32 and is useful for diagnosis of this defect.

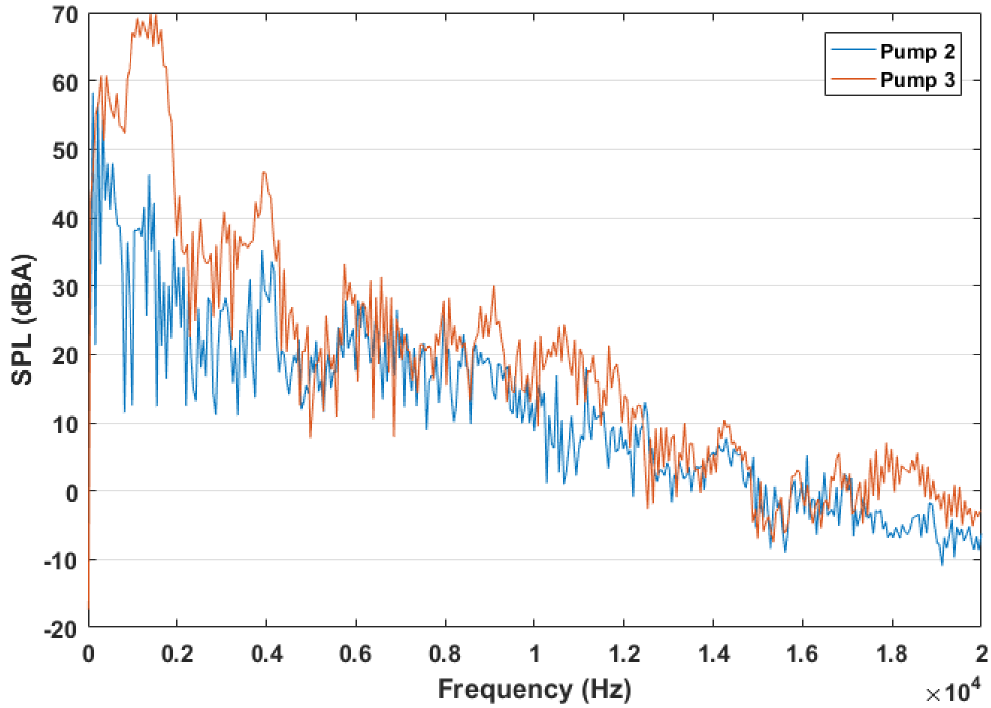

Figure 43: Envelope plot of missing washer pump compared to normal pump 12psi not controlled

Figure 43 is a plot of a pump that was missing a washer on one diaphragm and a spec pump operating under the same conditions (12 psi back pressure without motor control). The elevated acoustic envelope exhibited by the missing washer pump between 1000 and 2000 Hz is very similar to the trend of the missing washer plot in Figure 42. Above 5000 Hz there is very little difference between the two acoustic signatures.

CONCLUSIONS

Pump Acoustics

The acoustic signatures of the spec pumps were very similar from test to test. Though pump acoustic envelopes were similar between trials of the same conditions (pressure and motor control) varying a single condition resulted in a significant difference of acoustic output. Spec pumps that were operating with back pressure resulted in high peaks below 1000 Hz, while pumps operating in ambient conditions tended to have larger acoustic magnitudes that were centered around 2000 Hz. Regardless of pump test conditions the majority of the acoustic energy was propagated at lower frequencies. Spec pump acoustics held similar shape between trials of the same conditions, however, magnitudes of the pressure waves at certain frequencies could shift by up to +/- 10 dBA.

The defect orientation investigation sought to identify if there were different acoustics from a defect introduced on different sided of the duel diaphragm pump. It was concluded that there was no acoustic difference observed between trials with defects on opposing sides of a pump. Though Figure 19 does seem to contain a noticeable difference, the hole in the diaphragm study found that this variability was commonplace with a hole in the diaphragm.

An investigation was conducted to determine if hole in the diaphragm angular position affected the produced acoustics. It was concluded that the quietest hole in the diaphragm position was when the hole was located at an angle of 0, refer to Figure 21 for clarification. This position was selected for the hole in the diaphragm testing to ensure that the quietest hole in the diaphragm would still be detected by the diagnostic tool.

Extra Diaphragm

The extra diaphragm testing did not produce noticeable acoustical differences when compared to spec pump testing. Though Figure 36 did show a slightly increased acoustic output in the higher frequency ranges, the level of increase was within the variable limits of the spec pump acoustic envelope. Without definitive acoustic data to diagnose an extra diaphragm a secondary source was investigated, the rotational frequency.

When the pump speed was not controlled the pump operated full bore, or at maximum speed. The addition of an extra diaphragm increased the elastic “spring” effect of the diaphragm forcing the piston arms to work harder while actuating the diaphragm. This increase in motor work caused the pump to operate at lesser speeds. When a pump had an extra diaphragm and was pumping air against back pressure, the maximum rotational velocity achieved was 52.37 Hz. All spec 12 psi testing without speed control resulted in rotational velocities above 54 Hz. Though there was a lack of definitive acoustic evidence when an extra diaphragm was included in a pump, it was observed that the defect was still diagnosable by pump operating characteristics. Table 1 displays the values for the rotational rate of the motors with and without the presence of an extra diaphragm.

Table 1: Rotational speed of 12psi back pressure testing without motor control

Pump	12psi spec testing speed	12psi Extra Diaphragm Testing Speed
1	54.07	49.99 and 50.65
2	54.96	52.37 and 52.31
3	54.27	49.15 and 50.06
4	54.35	52.30 and 50.99
5	54.36	51.83 and 49.84
6	55.15	50.08 and 51.56

Because the acoustics did not signal if an extra diaphragm was present in the pump under test, the quality inspection tool testing parameters were narrowed to pumps operating under 12 psi back pressure without motor control. The backpressure and extra diaphragm added enough resistance to decrease the rotational speed of the pump significantly. The diagnostic tool used the lowered rotational speed (below 52.5 Hz) of a pump operating full bore as a diagnostic check for an extra diaphragm. Figure 44 displays the diagnostic procedure for pumps with an extra diaphragm.

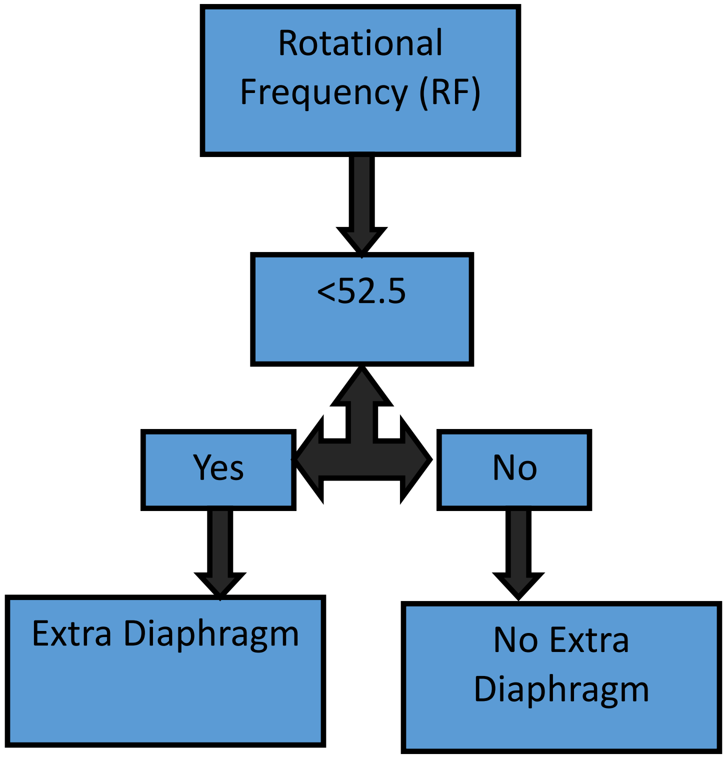

Figure 44: Diagnostic process for an extra diaphragm

Hole in Diaphragm

The introduction of a hole in the diaphragm of a pump specimen caused a large increase in the variability of the pump acoustics. This acoustic variability may be resultant of the utilization of different diaphragms. To increase the likelihood that diaphragm holes of different properties are covered by the quality inspection machine eight different diaphragm samples with holes were tested. If the shape and width of a specific tear in a diaphragm were different from another the resulting acoustics were affected.

Two distinct trends were noted in the acoustics for pumps with holes introduced to their diaphragm. The first trend was that the pump acoustic envelope looked very similar to a spec pump acoustic envelope making a diagnosis difficult. The second trend was that there was a large increase in audible waves after 7000Hz. The trends may have varied with the amount that the diaphragm washer contacted the diaphragm tear. If a washer covered the tear, pressure did not escape decreasing the amount that the pump acoustics are altered. Figure 38 displays a good depiction of the two hole in the diaphragm trends that were observed in the study.

With one acoustic peak trend (trend 1) indistinguishable from a spec pump acoustic peaks a diagnosis may only be reached for trend 2 pumps. Upon further investigation of the raw FFT of the pump acoustics a distinct behavior was noticed. The pump acoustic floor, or the acoustic energy that did not propagate as multiples of the rotational frequency, was elevated between 1000 Hz and 2000 Hz for pumps with holes in the diaphragm. This behavior can be observed in Figure 39 and Figure 41. The envelope plot traced together the peaks values and did not take into account the increase in the acoustic floor, thus sheltering the phenomena. A pump that has a tear or hole in one of its diaphragm will have an increase in the mean acoustic pressure over the 1000 Hz to 2000 Hz frequency range.

A comparison of mean acoustic pressure waves is used to diagnose a hole in the diaphragm. Comparing the mean acoustics between 0 and 1000 Hz to the mean acoustics between 1000 and 2000 Hz will signal if there is the telltale shift in the acoustic floor. The frequency spectrum is split into two ranges: indices 0 to 3906 and indices 3906 to 7812 corresponding to 0 to 1000 Hz and 1000 to 2000 Hz. Averages are calculated of the pressure magnitude over the corresponding windows. The averages are then compared and if there is a difference greater than 11 dBA the hole in the diaphragm indicator signals that there is a defect. The process for ensuring the diaphragm quality can be viewed in Figure 45.

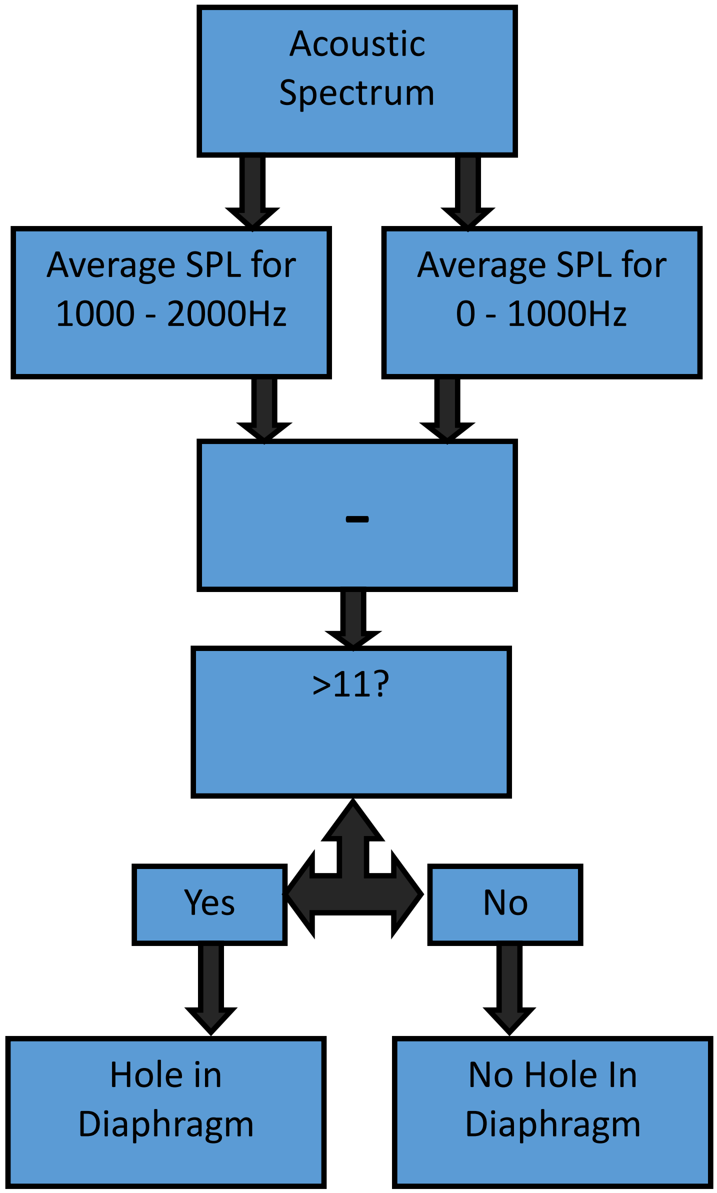

Figure 45: Diagnostic process for a hole in the one pump diaphragm

Missing Washer

The missing washer tests displayed the most obvious change in the acoustic signature of the pump. Every testing condition that the pump operated under resulted in a large acoustic energy spike between 500 and 2000 Hz. A standard pump's highest peaks under back pressure were below 1000 Hz and the trend was a gradual decrease at frequency increased. A pump with a missing washer displayed a large jump in the acoustic magnitudes after the initial peak.

Omitting a washer is a drastic change in the mechanical workings of the pump, which resulted in large changes of the lower frequency content of the spectrum. Acoustic magnitudes above 61 dBA within the lower acoustic frequency range (below 2000 Hz) is an indicator that a washer has been omitted during pump production. The full diagnostic procedure for a missing washer check can be viewed in Figure 46.

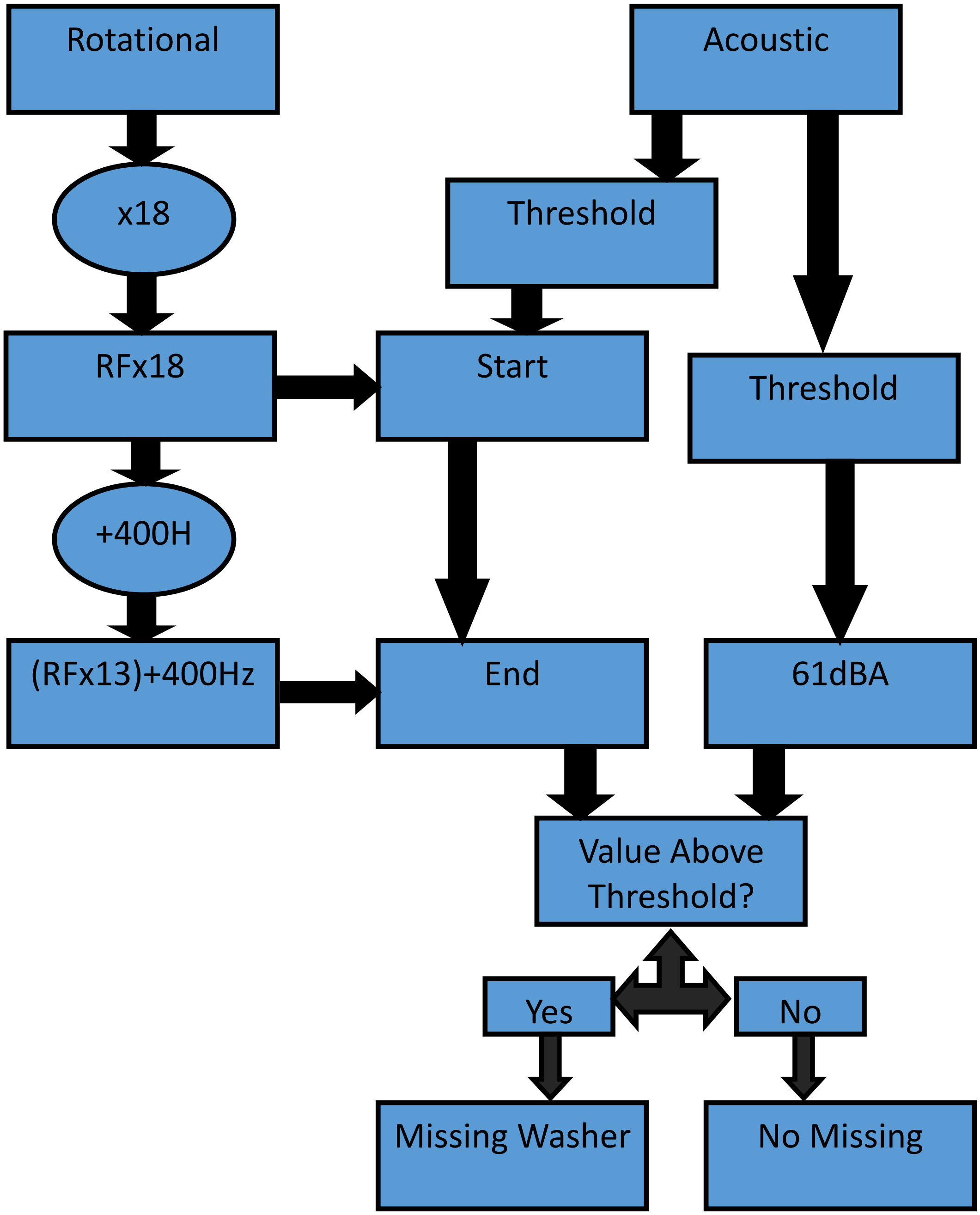

Figure 46: Diagnostic process for missing washer

The location of the large increase in acoustic energy appeared to shift with increases and decreases in the rotational rate of the motor. The large spike usually appeared at the 18th multiple of the rotational frequency. To account for this, the pump speed is measured and multiplied by 18 resulting in the frequency of the desired threshold testing location. The frequency is then divided by the frequency resolution to determine which element number corresponds to the starting frequency. This element number is used as the starting location of the threshold test.

Using the threshold tool described in the LabVIEW Diagnostic Process section the quality inspection tool will determine the expected location of the increased mechanical noise where a threshold is set at 61 dBA. The threshold window of interest is set to check 1538 elements for a SPL value over the threshold. If a peak exists above 61 dBA the diagnostic tool will signal that a washer is missing from the pump.

The increase in acoustic energy at 18x the rotational rate of the motor will also report a positive diagnosis for a hole in the diaphragm. A hole in the diaphragm, however, will not reach levels above the set threshold of 61 dBA. In order to halt the machine from diagnosing a missing washer as both a hole in the diaphragm and a missing washer a select tool is implemented. The tool is set to cut the display of the hole in the diaphragm indicator if the pump tested positive for a missing washer.

Thesis Goal Review

Four distinct goals were agreed upon at the proposal of this thesis: Diagnose three different pump defects based on the acoustic signature, Note similarities in acoustic signatures for certain defects, Design a prototype virtual instrument and test setup to diagnose pump defects introduced during the pump assembly, and to be able to alter the virtual instrument to inspect other machines.

All six pumps were tested after the introduction of three different defects. The defects were tested on each side of the pump to ensure defect orientation did affect the acoustic differences. Each of the six pumps with defects introduced were tested under 4 sets of operating conditions. Once a specific defect testing was completed the pumps were reassembled and tested to ensure that the reconstruction process did not alter acoustics.

The second goal was to note acoustic differences between the spec pump acoustic signatures and the defect pump acoustic signatures. The missing washer pumps displayed a notable increase in the acoustics between 500 and 2000 Hz. The missing washer also produced the loudest acoustic spikes in the study. Hole in the diaphragm tests often displayed a large difference in acoustic signature, however, some tests displayed very similar acoustic to those of a spec pump. When averaging the “noise floor” between 0-1000Hz and 1000-2000Hz it was noted that a hole in the diaphragm displayed an increase in energy propagating between 1000 and 2000Hz. Using an average value over these frequency ranges allowed for hole in the diaphragm acoustics to be distinguished from spec pump acoustics. Pumps with extra diaphragms did not produce noticeably different acoustics. The addition of an extra diaphragm increased the mechanical load on the motor but did not affect the acoustic output of the pump. To overcome the lack of acoustical difference the rotational speed of the pump was employed. If the motor (without speed control) did not achieve a speed greater than 52.5 cycles per second, an extra diaphragm was present.

To satisfy the third and fourth goal a prototype was made as a LabVIEW virtual instrument. The VI used an average comparison to diagnose a hole in the diaphragm, a threshold check to diagnose a missing washer, and a rotational rate assessment to determine if an extra diaphragm was accidentally installed. The VI can be altered to diagnose faults in other machinery by altering the locations that the threshold and mean SPL assessments are conducted. Acoustic divergences can be obtained by assessing baseline acoustics of machines to be inspected and comparing with acoustics of the machine with known defects. After the locations of certain divergences in acoustic signatures are obtained, the virtual instrument can have the window of the threshold check or the mean SPL comparison check altered for quality inspection of the new machine.

REFERENCES

Akay, A. (2002). Acoustics of friction. *Journal of the Acoustical Society of America, 111*(4), 1525-1548. doi:10.1121/1.1456514

Atalla, N., Panneton, R., Sgard, F., & Olny, X. (2001). Acoustic absorption of macro-perforated porous materials. *Journal of sound and vibration, 243*(4), 659-678.

Bollas, K., Papasalouros, D., Kourousis, D., & Anastasopoulos, A. (2013). Acoustic emission monitoring of wheel sets on moving trains. *Construction and Building Materials, 48*, 1266-1272.

Browne, A., & Paustian, A. (2016). *NOISE REDUCTION IN MEDICAL DIAPHRAGM PUMP USING VIBRATIONAL AND ACOUSTICAL ANALYSIS*. Paper presented at the Vibration Institute Annual Training Conference.

Bruel, & Kjaer. Typical randon-field responce with random incidence corrector. Prepolarized Free-field 1/2-inch Microphone Type 4936 specifications.

Carley, M. (2011). Turbulence and Noise. Online: University of Bath.

Chia Chen, C., Jung-Ryul, L., & Hyung-Joon, B. (2008). Structural health monitoring for a wind turbine system: a review of damage detection methods. *Measurement Science and Technology, 19*(12).

Elliott, R. (2006). Frequency and Amplitude Explained. *Elliott Sound Products.*

FFT Fundamentals (Sound and Vibration Measurement Suite). (2009). *Support Manuals.*

Grabowski, K., Gawronski, M., Nakatani, H., Packo, P., Baran, I., Spychalski, W., . . . Kundu, T. (2015, Mar 09-12). *Distance-domain based localization techniques for acoustic emission sources: a comparative study.* Paper presented at the Health Monitoring of Structural and Biological Systems, San Diego, CA.

Habel, W., & Heidmann, G. (2013). Electric Power Stations and Transmission Networks *Handbook of Technical Diagnostics* (pp. 471-504): Springer.

Hafizi, Z. M., Nizwan, C. K. E., Reza, M. F. A., & Johari, M. A. A. (2011). High Frequency Acoustic Signal Analysis for Internal Surface Pipe Roughness Classification. *Experimental Mechanics and Materials, 83*, 249-254. doi:10.4028/www.scientific.net/AMM.83.249

Han, F., Seiffert, G., Zhao, Y., & Gibbs, B. (2003). Acoustic absorption behaviour of an open-celled aluminium foam. *Journal of Physics D: Applied Physics, 36*(3), 294.

Harris, F. J. (1978). On the use of windows for harmonic analysis with the discrete Fourier transform. *Proceedings of the IEEE, 66*(1), 51-83.

Katabi, D., Hassahieh, H., Indyk, P., Price, E., Kapralov, M., & Shi, L. (2011). SFFT: Sparse Fast Fourier Transform. Retrieved from http://groups.csail.mit.edu/netmit/wordpress/projects/sparse-fourier-transform/

Kinsler, L., Frey, A., Coppens, A., & Sanders, j. (2000). *Fundamentals of Acoustics* (S. Johnson & B. Russiello Eds. fourth ed.): Publication Services, Inc.

Lu, B., Li, Y., Wu, X., Yang, Z., & Applications, I. P. E. a. M. i. W. (2009). A review of recent advances in wind turbine condition monitoring and fault diagnosis. 1-7.

Mba, D., & Rao, R. B. (2006). Development of Acoustic Emission Technology for Condition Monitoring and Diagnosis of Rotating Machines; Bearings, Pumps, Gearboxes, Engines and Rotating Structures.

Meissner, M. W., & Czechowicz, M. R. (1995). Experimental investigation of flow-induced acoustic oscillations in a piping system with closed branches. *Applied Acoustics, 45*(4), 359-375. doi:http://dx.doi.org/10.1016/0003-682X(94)00008-J

Meyer, E., & Neumann, E.-G. (1972). *Physical and Applied Acoustics*. New York and London: Academic Press.

Nored, M., Tweten, D., & Brun, K. P. D. (2011). COMPRESSOR STATION PIPING NOISE: NOISE MECHANISMS AND PREDICTION METHODS Gas Machinery Research Council Southwest Research Institute®.

Peake, N., & Parry, A. B. (2012). Modern Challenges Facing Turbomachinery Aeroacoustics. In S. H. Davis & P. Moin (Eds.), *Annual Review of Fluid Mechanics, Vol 44* (Vol. 44, pp. 227-248). Palo Alto: Annual Reviews.

Piercy, J. E., Embleton, T. F. W., & Sutherland, L. C. (1977). REVIEW OF NOISE-PROPAGATION IN ATMOSPHERE. *Journal of the Acoustical Society of America, 61*(6), 1403-1418. doi:10.1121/1.381455

Raišutis, R., Jasiūnienė, E., Šliteris, R., & Vladišauskas, A. (2008). The review of non-destructive testing techniques suitable for inspection of the wind turbine blades. *Ultragarsas (ultrasound), 63*(1), 26-30.

Shiotani, T., Oshima, Y., Goto, M., & Momoki, S. (2012). Damage identification of PC cable breakage by means of acoustic emission. *Emerging Technologies in Non-Destructive Testing V*, 95.

Takahashi, D. (1997). A new method for predicting the sound absorption of perforated absorber systems. *Applied Acoustics, 51*(1), 71-84. doi:http://dx.doi.org/10.1016/S0003-682X(96)00070-9

Tweten, D., Nored, M., & Brun, K., Ph.D. (2008). *The Physics of Pulsations*. Paper presented at the Gas Machinery Conference.

Understanding FFTs and Windowing. (2015). *Instrument Fundamentals.*

Vandamme, L. (1994). Noise as a diagnostic tool for quality and reliability of electronic devices. *Electron Devices, IEEE Transactions on, 41*(11), 2176-2187.

Weisstein, E. W. (2002). Discrete fourier transform.

Zhao, X., & Fan, X. (2015). Enhancing low frequency sound absorption of micro-perforated panel absorbers by using mechanical impedance plates. *Applied Acoustics, 88*, 123-128. doi:http://dx.doi.org/10.1016/j.apacoust.2014.08.015

APPENDIX A: GRAPHS

Appendix 1

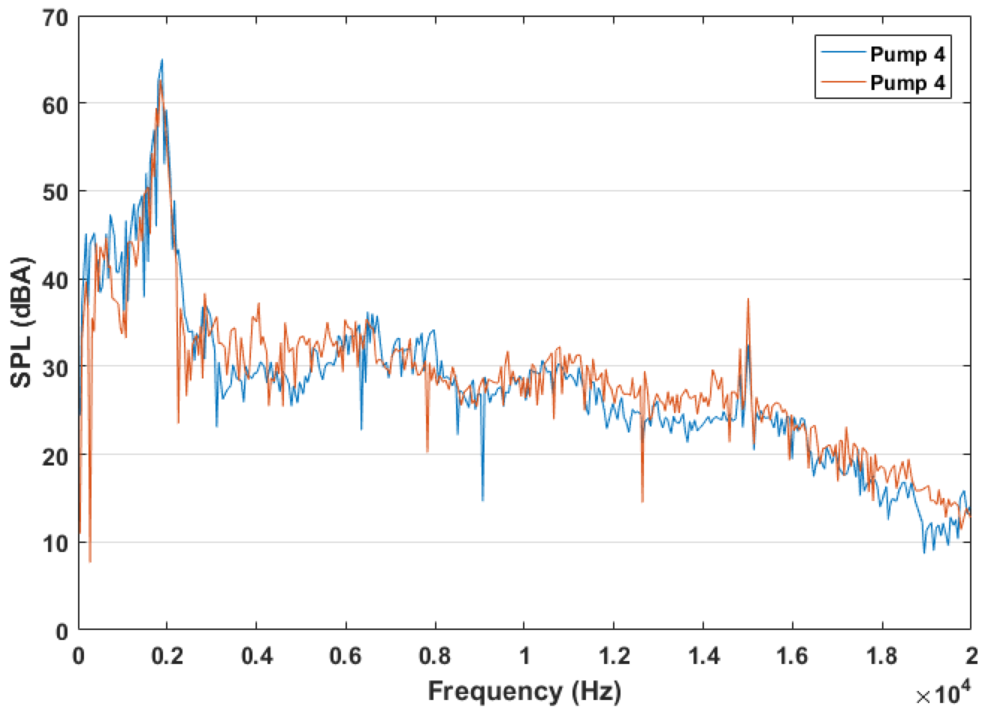

Figure 47: Envelope plot of extra diaphragm pump compared to normal pump ambient controlled

Appendix 2

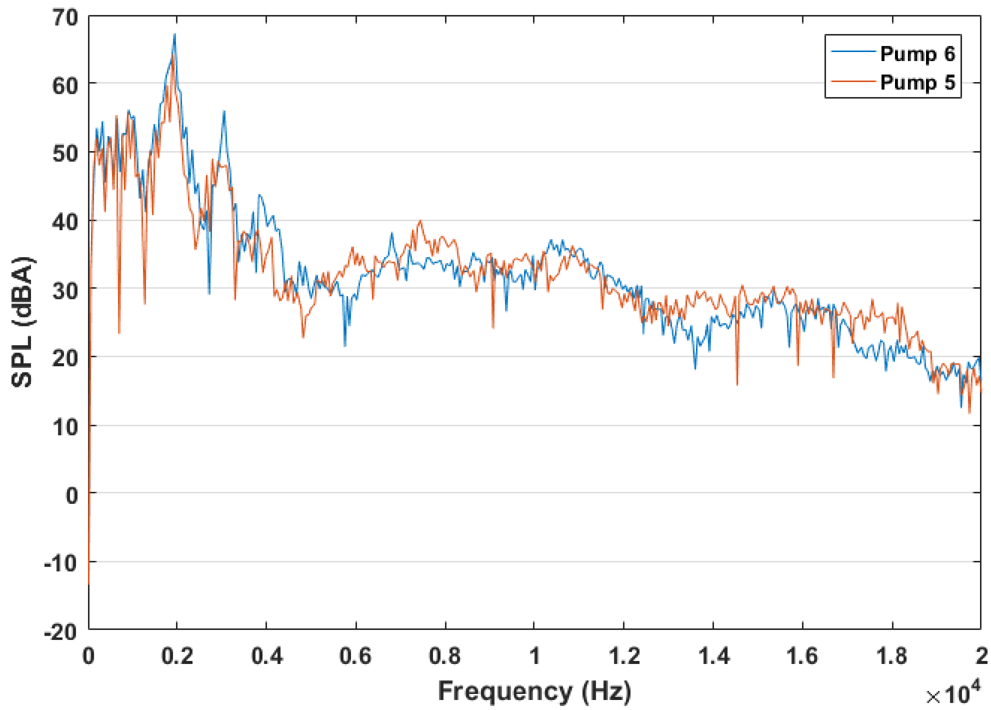

Figure 48: Envelope plot of extra diaphragm pump compared to normal pump ambient not controlled

Appendix 3

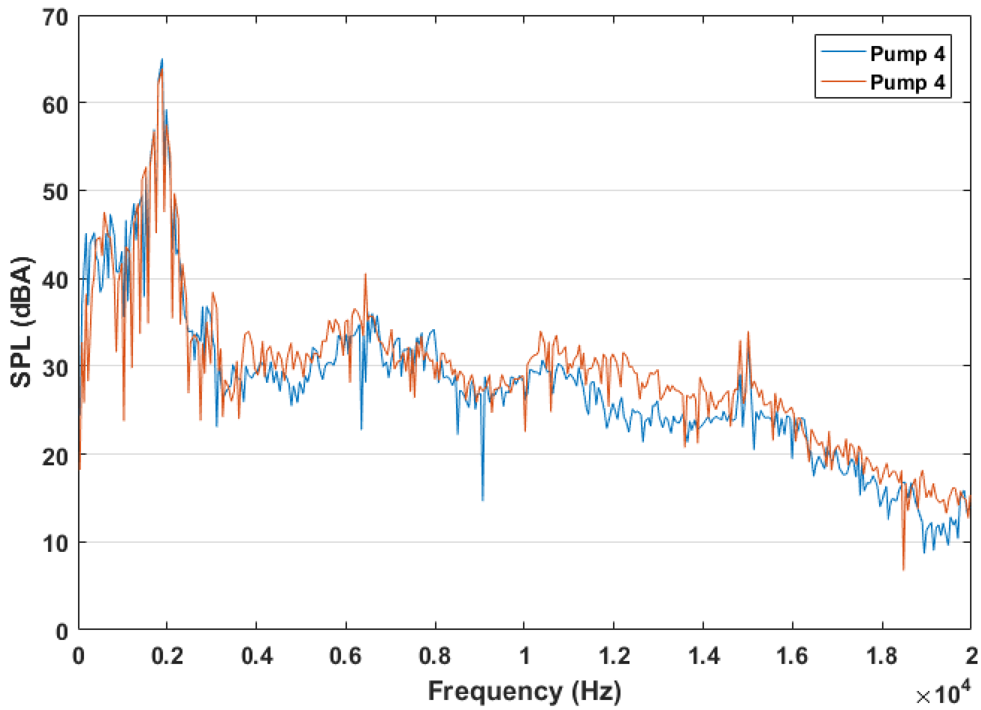

Figure 49: Envelope plot of hole in diaphragm pump compared to normal pump ambient controlled

Appendix 4

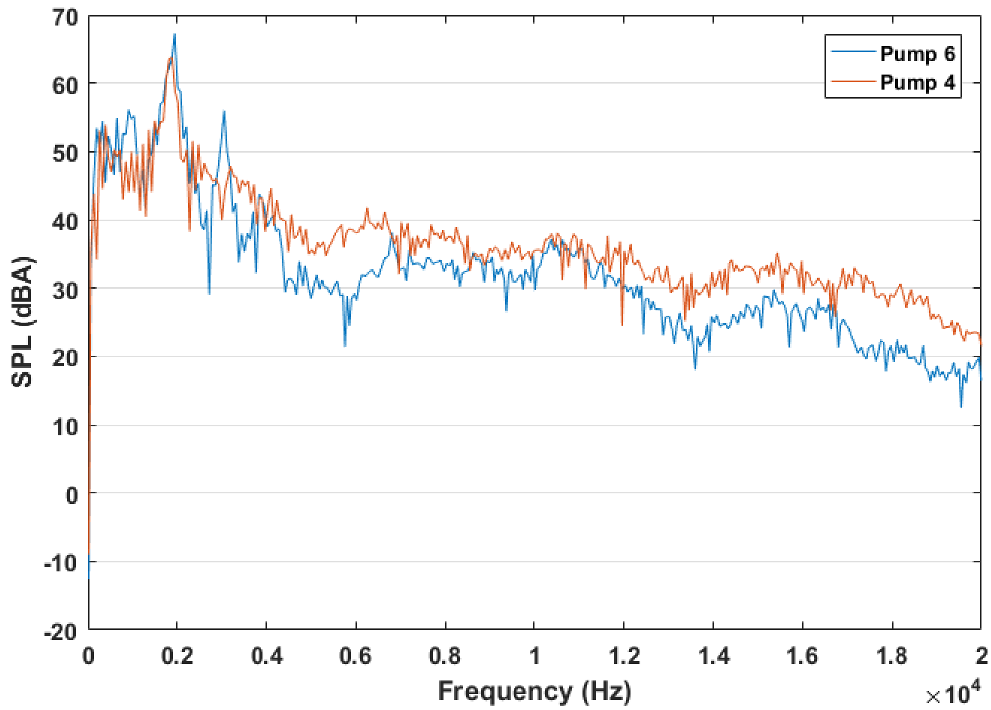

Figure 50: Envelope plot of hole in diaphragm pump compared to normal pump ambient not controlled

Appendix 5

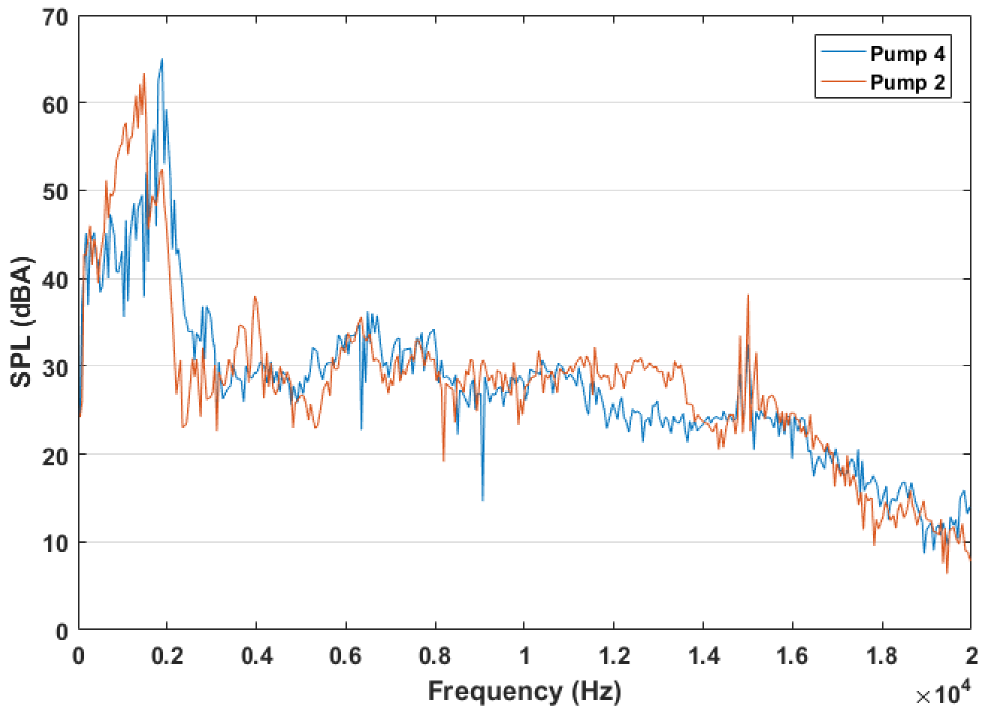

Figure 51: Envelope plot of missing washer pump compared to normal pump ambient controlled

Appendix 6

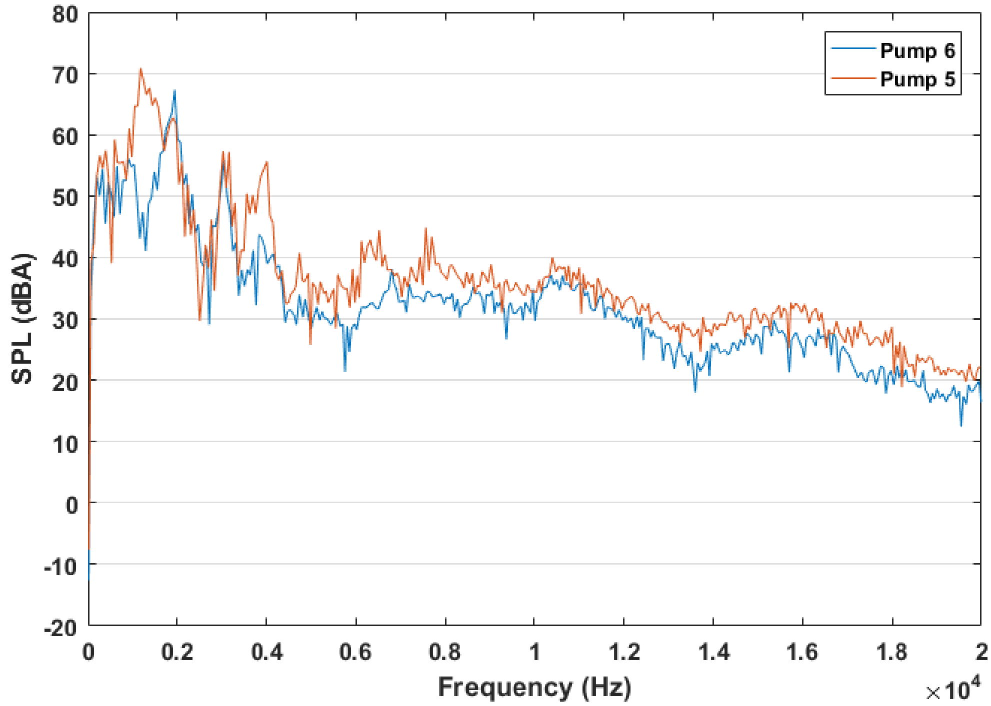

Figure 52: Envelope plot of missing washer pump compared to normal pump ambient not controlled

Appendix 7

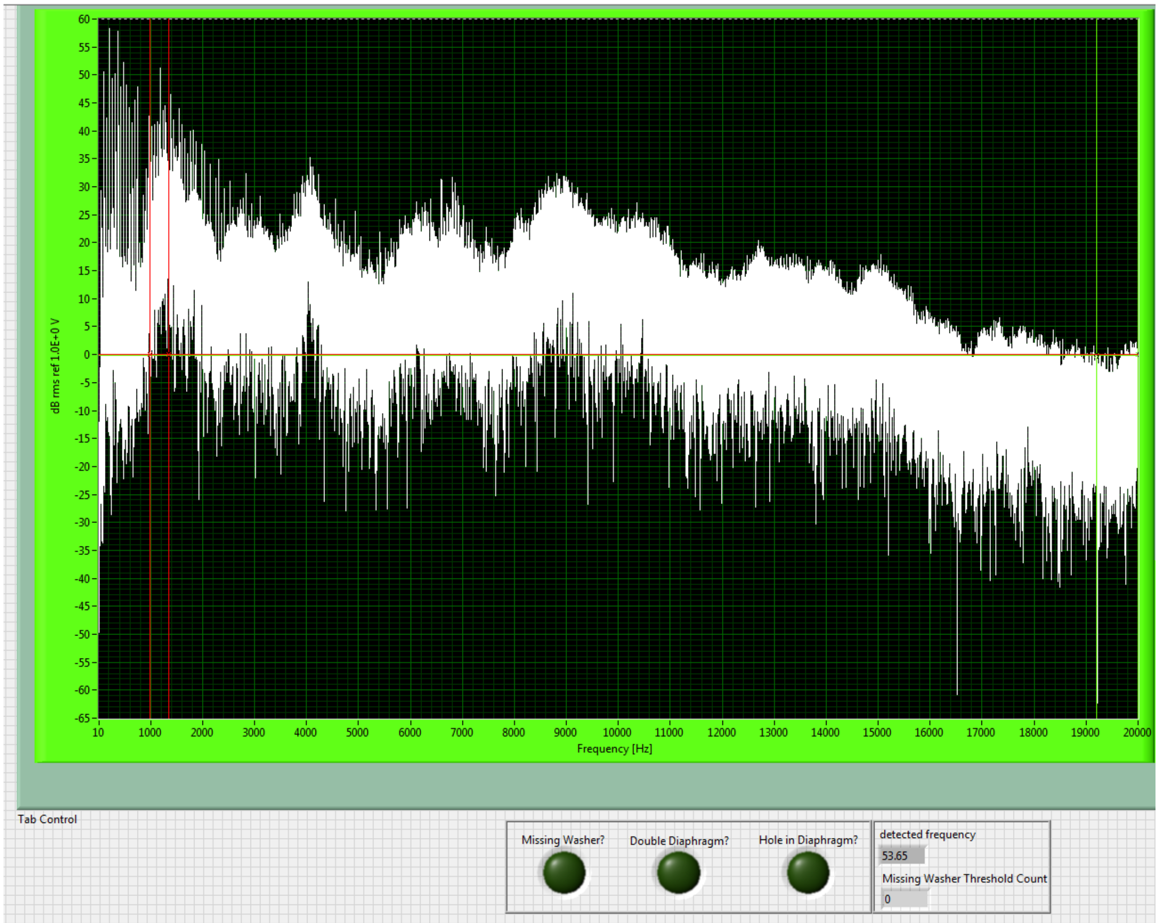

Figure 53: Front panel of the LabVIEW virtual instrument

Appendix 8: MATLAB envelope tool

```
if qfiles > 0
    [Peaks1,Freq1] =
findpeaks(Pump(:,1),Frequency(:,1),'MinPeakDistance',45);
end
if qfiles > 1
    [Peaks2,Freq2] =
findpeaks(Pump(:,2),Frequency(:,2),'MinPeakDistance',45);
end
if qfiles > 2
    [Peaks3,Freq3] =
findpeaks(Pump(:,3),Frequency(:,3),'MinPeakDistance',45);
end
if qfiles > 3
    [Peaks4,Freq4] =
findpeaks(Pump(:,4),Frequency(:,4),'MinPeakDistance',45);
end
if qfiles > 4
    [Peaks5,Freq5] =
findpeaks(Pump(:,5),Frequency(:,5),'MinPeakDistance',45);
end
if qfiles > 5
    [Peaks6,Freq6] =
findpeaks(Pump(:,6),Frequency(:,6),'MinPeakDistance',45);
end

if qfiles > 0
    plot(Freq1,Peaks1)
    title('2-D Line Plot')
    xlabel('Frequency')
    ylabel('dBA')
end
hold on
if qfiles > 1
    plot(Freq2,Peaks2)
end
hold on
if qfiles > 2
    plot(Freq3,Peaks3)
end
hold on
if qfiles > 3
    plot(Freq4,Peaks4)
end
hold on
if qfiles > 4
    plot(Freq5,Peaks5)
end
hold on
if qfiles > 5
    plot(Freq6,Peaks6)
end
```